Nuclear structure along the $Z = 28$ and $Z = 50$ shells

Shell evolution and shape coexistence in ^{74,76,78}Cu and ^{126}Sn

Line Gaard Pedersen

Supervisors:
Andreas Görgen
Eda Sahin

Department of Physics

Faculty of Mathematics and Natural Sciences

Series of dissertations submitted to the
Faculty of Mathematics and Natural Sciences, University of Oslo
No. 2719

ISSN 1501-7710

Cover: UiO.
Print production: Graphic center, University of Oslo.

Abstract

This thesis presents the nuclear structure studies of nuclei near the $Z = 28$ and $Z = 50$ shell closures, presenting case studies of the odd-odd nuclei ^{74,76,78}Cu and the even-even nucleus ^{126}Sn. Level schemes are presented for ^{74,76,78}Cu for the first time, shedding light into the Cu isotopic chain as well as the Ni isotopic chain, and providing information on the proton-neutron interaction for neutron-rich Cu isotopes near doubly magic ^{78}Ni. Data on ^{74,76,78}Cu are obtained by fission-induced β decay of ^{74,76,78}Ni, performed at the RIKEN Nishina Center during the EURICA campaign. In ^{126}Sn, an excited 0^+ state is observed for the the first time through a two-neutron transfer reaction experiment performed at IFIN-HH. With excited 0^+ intruder states observed for all even Sn isotopes between ^{110}Sn and ^{124}Sn, the newly observed excited 0^+ state in ^{126}Sn is the next step in the shape coexistence studies along the Sn isotopic chain. Isotopic chains along shell closures serve as important benchmarks for nuclear structure studies, and the experimental results presented in the thesis are compared to shell model calculations where possible.

Sammendrag

Denne avhandlingen omhandler kjernestruktur nær de magiske tallene $Z = 28$ og $Z = 50$ og presenterer studier av odd-odd kjernene ^{74,76,78}Cu og like-like kjernen ^{126}Sn. Nivåskjema er for første gang presentert for ^{74,76,78}Cu, som gir mer innsikt i både rekken av Cu-isotoper og Ni-isotoper nær den dobbelt-magiske kjernen ^{78}Ni. ^{74,76,78}Cu-data er tatt ved fisjon-indusert β-henfall fra ^{74,76,78}Ni i et eksperiment på RIKEN Nishina Center under EURICA-kampanjen. En eksitert 0^+-tilstand er observert for første gang i ^{126}Sn gjennom et to-nøytron-overføringseksperiment gjennomført på IFIN-HH. 0^+ intrenger-tilstander er tidligere observert for alle like-like Sn-kjerner fra ^{110}Sn til ^{124}Sn, og den nyobserverte 0^+-tilstanden i ^{126}Sn er det neste steget i studiet over sameksistens av former gjennom rekken av Sn-isotoper. Isotop-rekker langs skallgap er viktige for kjernestruktur-studier og de eksperimentelle resultatene fremlagt i denne avhandlingen er sammenlignet med skallmodelberegninger der dette har vært mulig.

Contents

List of Figures

List of Figures

List of Tables

Preface

Acknowledgements

I want to thank my supervisors, Andreas Görgen and Eda Sahin, for all your support over the past years. I first met you back in 2017 near the end of my bachelor and was captivated by the project you offered me that would become my master project and later develop into part of my PhD thesis. I feel very lucky to have been able to work with both of you for all these years. It has been a privilege to not only have two supervisors who I work well with, but who also work well together. Most of our meetings have included all three of us, and I am truly grateful for this cooperation. It really feels like we have been a great team with different strengths coming together in the best ways. In addition to all our physics discussions, you have also provided me with a sense of comfort and optimism through the harder times, from pandemic lockdowns to paper rejections. You have seen me cry many times, but also celebrated all the small victories along the way. Thank you for being with me through these past years. I realise what a privilege it is to be able to finish my PhD with only positive things to say about my supervisors in the end.

I also want to thank all the wonderful people at the Oslo nuclear physics group, who have given me so many happy memories. Whether it has been at conferences and summer schools abroad or sharing a break at the lunch room together, every one of you have added your unique vibe to the group and my days here.

Lastly, I want to thank my friends and family who have supported me through this PhD. It has been great to be able to vent about my inevitable frustrations or keep my mind busy with other things in your presence. Thank you for hanging out with me and for your patience with me. I especially want to give a shout out to Kristine. When I no longer could see you everyday at work, I had no choice but to move in with you to keep your wonderful presence in my life as much as I wanted. Thank you for all your support and patience, both while working together and as a flatmate. I promise to get better at cleaning the kitchen now.

Part I

Introduction to nuclear structure and the papers

Chapter 1

Introduction

1.1 Nuclear structure

Nuclear science has come a long way since the discovery of the basic structure of atoms, with protons and neutrons forming the atomic nucleus and electrons outside the nucleus. Nuclear physics is the study of the protons and neutrons making up the nucleus, and how these interact with each other. The shape and structure of a nucleus is governed by the number of protons and neutrons in the nucleus and the orbitals they occupy.

The atomic nucleus is a complicated many-body quantum system. There is yet not a single unifying theory that explains all characteristics exhibited by nuclei, and calculating different nuclear properties from first principles is only possible for the lightest nuclei with few protons and neutrons. Different nuclear models are therefore developed to simplify the many-body problem and to explain phenomena observed across the nuclear chart.

At the quantum scale, only specific energies are allowed for the nucleus. Illustrations of the various quantum states in a nucleus with their energies, spins and parities, and the decay pattern between them are called nuclear level schemes. In colloquial terms, this can be seen as the finger print of the nucleus as every nucleus has its own unique level scheme. In addition to describing the various energies of the nucleus, the level scheme can also give unique insight into different nuclear properties.

The total energy of the nucleus is determined by the energies of the orbitals that the protons and neutrons occupy, and by the interactions between the nucleons. As protons and neutrons are fermions, only certain numbers of them are permitted to occupy specific orbitals, following the Pauli principle. The nuclear shell model describes the occupation and interaction of nucleons in the various orbitals that are characterised by their angular momentum and parity. A schematic drawing of the shell model is shown in Figure 1.1. Between some of the orbitals there are larger energy gaps, indicating that more energy is needed to excite a nucleon to the next orbital. These large shell gaps are called magic numbers, and indicate that nuclei with these specific numbers of protons or neutrons are more tightly bound.

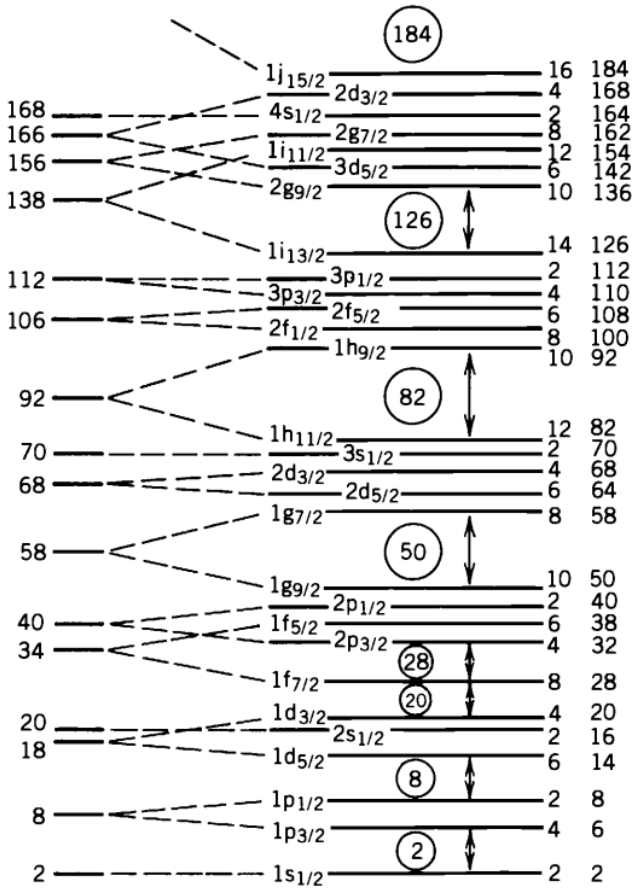

Figure 1.1: The shell model illustrates the different nucleon orbitals. Numbers to the right of the orbital labels say how many nucleons fit in each orbital, and in total up to each orbital. Circled numbers illustrate the magic numbers and correspond to how many nucleons can be filled up to the orbital in question. Figure obtained from [1].

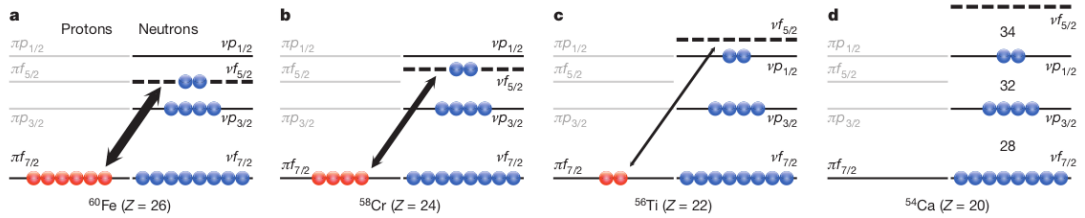

Figure 1.2: Illustration of the tensor force between the $\pi f_{7/2}$ and $\nu f_{5/2}$ orbitals, pushing the neutron orbital as protons are removed from the proton orbital. As the $\nu f_{5/2}$ orbital gets pushed up in energy, both $N = 32$ and $N = 34$ emerge as semi-magic numbers in ^{54}Ca. Figure obtained from [7].

The traditional magic numbers, as presented in Figure 1.1, were all first discovered for nuclei close to stability. They can be calculated by using a modified harmonic oscillator potential and adding an angular momentum term proportional to l^2 and spin-orbit coupling term proportional to $\vec{l} \cdot \vec{s}$, as first shown in Refs. [2, 3]. With these terms, all magic numbers that were observed experimentally in nuclei close to stability could be calculated correctly. However, after eventually gaining more knowledge on nuclei far from stability, it became apparent that some magic numbers break down far from stability, while new magic numbers emerge. Examples include the breaking of the $N = 8, 20, 28$ magic numbers at the so-called islands of stability [4–6]. Similarly, the semi-magic numbers $N = 32$ and $N = 34$ were seen to appear in ^{54}Ca [7]. Compared to the shell model as illustrated in Figure 1.1, this is explained by the $\nu f_{5/2}$ orbital being pushed up in energy when protons are removed. Eventually the $\nu f_{5/2}$ crosses the $\nu p_{1/2}$ orbital, leaving a larger energy gap between the $\nu p_{1/2}$ and $\nu p_{1/2}$ orbitals, and creating a new shell gap between the $\nu p_{1/2}$ and $\nu f_{5/2}$ orbitals. This is illustrated in Figure 1.2. To explain this, yet another term is needed to correctly calculate the magic numbers that arise when moving away from stability. The tensor force was introduced as a robust general feature [8] which acts between single-particle orbitals of protons and neutrons. It is this tensor force which is responsible for the shell evolution along isotopic and isotonic chains.

The shell model is only one of the models used to simplify the nuclear many-body problem and to explain energy levels in nuclei, and is best suited to describe nuclei near closed shells (magic numbers). For other nuclei far from magic numbers, mean-field based and collective models are more appropriate. In this thesis, nuclei at or near closed shells are studied, and it is therefore this model that is in focus here.

As the effects of the tensor force are most clearly seen near shell closures, magic nuclei are important benchmarks when studying nuclear structure and deformation. This thesis is centred around two magic isotopic chains: the Sn chain along the $Z = 50$ magic number and the Cu chain, one proton away from the $Z = 28$ magic number. We will also look specifically into the structure near mid-shell between ^{100}Sn and ^{132}Sn and the neutron-rich side near the doubly magic nucleus ^{78}Ni.

1.1.1 Proton-neutron interactions

Each nucleon carries a given spin and parity based on which orbital it occupies. The short-range nature of the strong nuclear force favours antiparallel coupling, and a proton-proton or neutron-neutron pair in the same orbital will couple together with antiparallel alignment to spin 0. In an even-even nucleus, i.e. a nucleus with even numbers of both protons and neutrons, the ground state will therefore always be 0^+. In an odd-odd nucleus, where there is an odd number of both protons and neutrons, the two unpaired nucleons of each type will couple to each other. Since the nucleons are of different types, they are not bound by the Pauli principle, and can couple to different spins, giving all possible spins from parallel $|\vec{j_\pi}| + |\vec{j_\nu}|$ to antiparallel $|\vec{j_\pi}| - |\vec{j_\nu}|$. The proton-neutron interaction produces a multiplet of different states and spins. Because of these multiples, the ground state spin of an odd-odd nucleus is difficult to predict without experimental investigations.

When an orbital is almost filled, but not completely, it is sometimes convenient to think of the lack of particle as a 'hole', and describe the interactions with this hole. We then get a situation where an unpaired nucleon can couple to another nucleon (particle-particle), or to a hole (particle-hole). An empiric study of odd-odd nuclei across the nuclear chart has found parabolic trends for the energies of states belonging to a given spin multiplet as a function of $I(I+1)$ [9], where I is the total angular momentum of a given state, more conventionally called 'spin'. Because of the short range nature of the interaction, the two nucleons try to maximise their overlap, leading to parallel and antiparallel coupling being favoured. Plotting the energies along $I(I+1)$, this gives a negative parabola, with the highest and lowest spins energetically favoured. With a large difference in the preferred spins, there is a high probability to find isomeric states at low energies. In the particle-hole coupling case, the maximum overlap is gained from the perpendicular coupling. For the particle-hole coupling, we thus get a positive parabola with intermediate spins being energetically favoured.

Experimentally determined multiplets can be used to characterise the proton-neutron interaction. By experimentally measuring all the states in a multiplet relative to the ground state, we can translate the energy of each state into the binding energy if the mass is known. The total energies $E_I(j_\pi, j_\nu)$ for a given state of spin I with nucleons in orbitals j_π and j_ν, are called the Two-Body Matrix Elements (TBME). The spin-weighted TBME is called the monopole interaction, and is given as [10]

$$V^{pn}_{j_\pi j_\nu} = \frac{\sum(2I+1) \times E_I(j_\pi, j_\nu)}{\sum(2I+1)}. \tag{1.1}$$

This monopole interaction can be further broken down into three different components: the central part, the spin-orbit part, and the tensor part. The central part depends only on the relative distance between the two particles. The spin-orbit part depends on the orientation between the orbital angular momentum between the two particles and their intrinsic spin. Finally, the tensor part depends on the orientation of the distance vector and the intrinsic spin of the two particles.

It is the tensor part of the monopole interaction that is responsible for the

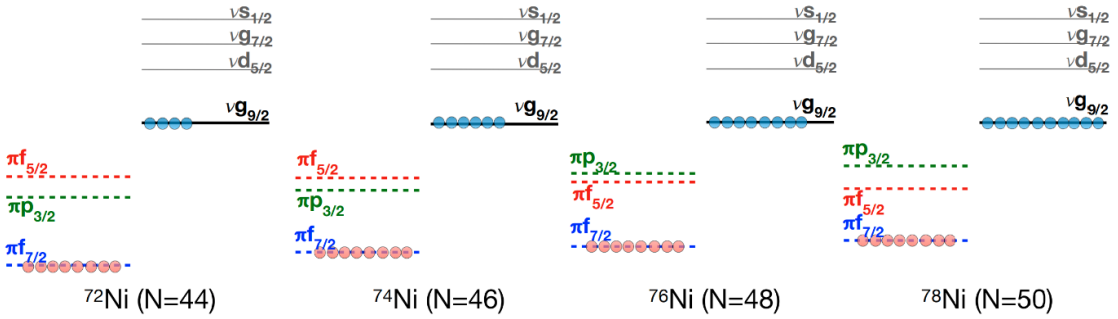

Figure 1.3: Illustration of the relative energies between the $\pi f_{5/2}$ and $\pi p_{3/2}$ orbitals. As more neutrons fill the $\nu g_{9/2}$ orbital, the relative energies of the $\pi f_{5/2}$ and $\pi p_{3/2}$ orbitals shift. The tensor interaction is repulsive between the $\pi p_{3/2}$ and $\nu g_{9/2}$ orbitals, pushing the $\pi p_{3/2}$ orbital up in energy, and attractive between $\pi f_{5/2}$ and $\nu g_{9/2}$, pulling the $\pi f_{5/2}$ orbital down in energy as the $\nu g_{9/2}$ orbital is filled. Figure from [14].

shell evolution when moving away from stable nuclei [8]. Using the neutron-rich odd-odd Cu isotopes as an example, the $\nu g_{9/2}$ ($l = 4, j = +\frac{1}{2}$) orbital gradually gets filled with neutrons for increasingly heavier isotopes. The unpaired neutron can couple to the unpaired proton either in the $\pi p_{3/2}$ ($l = 1, j = +\frac{1}{2}$) or in the $\pi f_{5/2}$ ($l = 3, j = -\frac{1}{2}$) orbital. The tensor force is repulsive if the proton and neutron have the same coupling between orbital angular momentum and spin, either $j = l + s$ or $j = l - s$, and attractive if they have the opposite coupling, one having $j = l + s$ and the other $j = l - s$. This leads to the $\pi p_{3/2}$ orbital being pushed up in energy and the $\pi f_{5/2}$ being pulled down in energy when adding neutrons to the $\nu g_{9/2}$ orbital.

With the increasing number of neutrons in the $\nu g_{9/2}$ orbital the effect of the tensor force on the $\pi p_{3/2}$ and $\pi f_{5/2}$ becomes so strong that the two orbitals cross each other for the heavier Cu isotopes. For an odd nucleus in its ground state, with a single unpaired proton or neutron, the whole spin of the nucleus will be given by the unpaired nucleon. The odd-even Cu isotopes from neutron-deficient, stable and up to neutron-rich ^{73}Cu all have ground state spin $3/2^-$, based on the single uncoupled proton in the $2p_{3/2}$ orbital. However, previous studies [11–13] have found that the odd-even Cu isotopes ^{75,77}Cu have a ground state spin of $5/2^-$, based on the uncoupled proton being in the $\pi f_{5/2}$ orbital. This indicates that with enough neutrons in the $\nu g_{9/2}$ orbital, the $\pi f_{5/2}$ orbital is pushed down in energy, and the $\pi p_{3/2}$ up in energy, enough to cross each other. The effect is illustrated in Figure 1.3. It is the same mechanism that explains the effect illustrated in Figure 1.2, where the $\nu f_{5/2}$ orbital is pulled down in energy when adding protons to the $\pi f_{7/2}$ orbital. In addition to being responsible for the new or disappearing magic numbers, the consequences of the tensor interaction can also be seen in the single-particle energies in odd-mass nuclei.

One accessible way to study proton-neutron interactions is by studying odd-odd nuclei, where the unpaired proton and neutron couple to each other (particle-particle) or an unpaired proton couples to a neutron hole (particle-hole). This will reveal the tensor interaction better, and can be used to fine-tune future shell model calculations even further from stability.

1.1.2 Shell Model Calculations

While experimental results are valuable on their own, the gain in understanding of the nuclear structure is greater when compared to theoretical calculations. It is when theoretical predictions and experimental results come together that we can gain the greatest knowledge, as the consistency between predictions and results can reveal more about how well our understanding is. A significant part of the papers in this thesis is therefore devoted to comparing the experimental results to calculations.

Atomic nuclei are complex, and when all particles interact with each other, the computation times scale exponentially for each particle added to the calculation. Ab-initio calculations, where all interactions are treated by first-principal physical forces, are therefore only currently possible for light nuclei with few nucleons. In order to overcome higher-dimension problems, it is necessary to simplify the calculations. Shell model (SM) calculations are one way of simplifying the many-body problem. In addition to restricting how many high-lying orbitals are included in the calculation, SM calculations also use an inert core that does not interact with any of the particles in the valence space. Doubly magic nuclei are often chosen as the inert core. In addition, it is possible to make further truncations by limiting the number of nucleons allowed to be excited to specific orbitals.

SM calculations are successful for relatively light nuclei, but not always for heavier cases that require larger model spaces or core-excited states. As they restrict or do not allow for single-particle excitation across shell gaps or intruder states, they can not be used to calculate nuclei with these types of excitations. To overcome this problem, Monte Carlo Shell Model (MCSM) calculations have been developed [15, 16], which apply Monte Carlo techniques to determine which configurations are most important and exclude less important configurations. MCSM calculations can thus calculate more complex problems than classical shell model techniques and include a larger number of valence orbitals compared to traditional SM calculations [17]. Specifically, it is possible to include more than one major shell in the valence space, allowing calculations of intruder states that are based on excitations across shell gaps. However, both the traditional and the Monte Carlo Shell Model require experimental input to be able to treat the interactions between the nucleons properly.

Any shell model calculation requires a model for the nucleon-nucleon interaction that is adapted to the model space. This is referred to as the *effective interaction*. The effective interaction can be obtained from the bare nucleon-nucleon interaction, or by fitting the single-particle energies and the TBME to experimental data. In order to refine these effective interactions, experimental results for the mass-region of interest are needed. This can both be used to estimate the validity of the theoretical calculations, and to improve calculations for even more unstable nuclei. For the Cu isotopic chain, the new data on ^{74,76,78}Cu are the most exotic experimental results on odd-odd nuclei in the ^{78}Ni-region. While previous experiments on the odd-even Cu isotopes have revealed single-particle structures that can be used to tune the SM calculations, the new results add important information about the proton-neutron interaction for the first time in this mass region.

In the shell model, the wave function is expanded in the basis of the single-particle orbitals. When the orbitals are close in energy, the wave function of a particle can be spread over multiple orbitals. One output of SM calculations are *occupation numbers*, which show how many protons or neutrons occupy the different orbitals. For 'clean' and well defined states, the occupation numbers are close to whole numbers for each orbital. If the numbers are not close to whole numbers, the states are said to be more mixed and the wave function is more spread.

1.1.3 Shape coexistence

Nuclei take on different shapes. While nuclei near closed shells generally have spherical shapes, nuclei with open shells usually gain energy by assuming a deformed shape. Prolate quadrupole shapes are the most common form of deformation, but in some cases oblate quadrupole shapes or octupole (pear) shapes are favoured. *Shape coexistence* refers to nuclei that can take on different shapes based on their energy level [18, 19]. In a strict sense, shape coexistence involves states that can be associated with distinct and well separated minima in the potential energy surface, and whose configurations do not strongly mix. However, mixing is generally present, and structures are often interpreted in terms of shape coexistence even in the presence of configuration mixing.

Shape coexistence appears in widely different nuclei across the entire nuclear chart, and different underlying dynamics appear to lead to shape coexistence in different regions [18]. Because of this variation in underlying mechanisms and the lack of a unified picture, the theoretical description of shape coexistence can be challenging. Shape coexistence lies in-between the single-particle and macroscopic pictures, as it can be driven by single-particle excitations but only seen specifically in the macroscopic picture.

The direct measurement of nuclear shapes is very difficult, and in some cases even impossible. It is therefore common practice to base arguments for shape coexistence on indirect, but more accessible measurements. Especially band structures, with their energy spacing and electromagnetic transition probabilities, often provide a first indirect indication for shape coexistence. In any case, spectroscopic 'fingerprinting' is of great importance to investigate and establish shape coexistence. Specific structures of the level schemes, especially γ-decay patterns between states, can be used to interpret the coexistence of shapes.

Another common argument for shape coexistence is the probability of populating specific states through different reactions. An example of this is the nucleon-pair transfer reaction at and near singly closed shells, which has been shown to effectively populate 0^+ excited states at relatively low energies.

Isotopic chains along the singly-closed shells have been shown to exhibit shape coexistence, with deformed excited 0^+ states with a deformed rotational band on top. A textbook example of this phenomenon is the Sn isotopic chain. With 50 protons, the Sn isotopic chain lies on a magic number, and at the neutron-rich and proton-rich sides we find doubly magic ^{100}Sn and ^{132}Sn. Excited 0^+ states are found in all even-even Sn isotopes from ^{110}Sn to ^{124}Sn, many of which carry

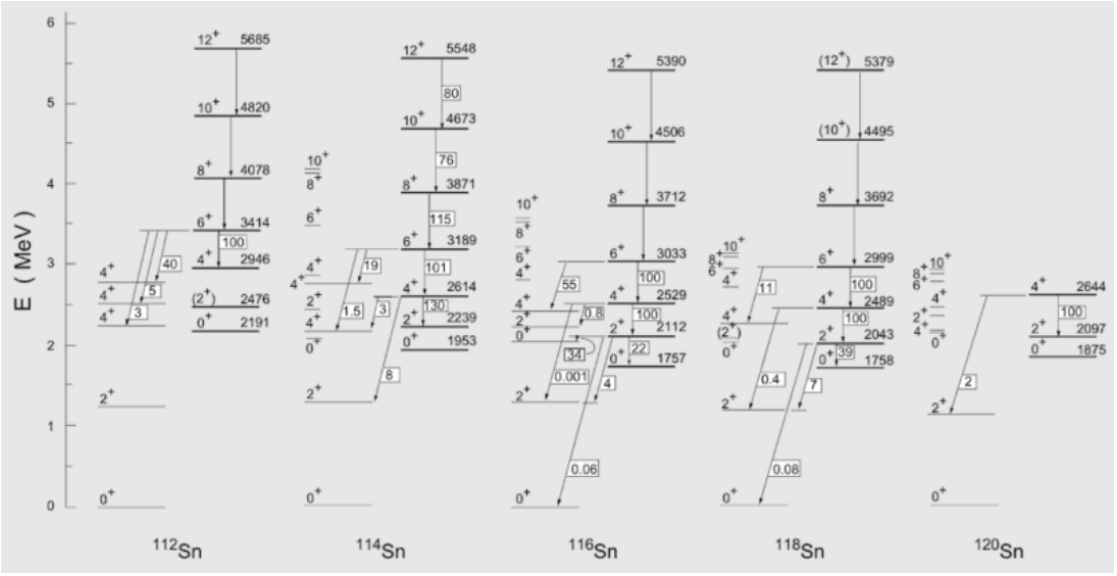

Figure 1.4: A literal textbook example, showing the development of the 0^+ excited intruder states in Sn with rotational bands on top. Obtained from D.J. Rowe and J.L. Wood, Fundamentals of Nuclear Models [21].

rotational bands on top. The rotational character of the bands built on the excited 0^+ states clearly suggests the presence of deformation. In addition, their strong population in two-proton transfer reactions supports their interpretation as two-proton-two-hole intruder states [20]. However, experimental data with evidence for this excited 0^+ state is missing for more neutron-rich nuclei from ^{126}Sn and the systematics across the entire shell is not yet completed. To shed more light on this we have studied ^{126}Sn. It is known that the energies of the 0^+ deformed states are lowest at mid-shell, but in order to properly understand how these evolve over the entire shell, data on more exotic Sn isotopes are needed.

Another closed shell isotopic chain is the Ni chain. Figure 1.5 shows the predicted 0^+ core excited states. For the neutron-rich Ni isotopes, the 0^+ state is known experimentally for only ^{68,70}Ni, which MCSM calculations predict to be 0^+ prolate intruder states. Only theoretical SM values were used in the Figure for the heavier Ni isotopes. The 0^+ excited states show the same parabolic structure as is seen in other closed-shell intruder states, indicative of shape coexistence. According to the calculations, the excited 0^+ states in Ni are based on particle-hole excitations across the $Z = 28$ shell gap. Their energies should therefore follow the same trend as the energies of the core-excited $\pi f_{7/2}$ states in Cu, with a hole in the $\pi f_{7/2}$ orbital. The figure compares the excitation energies of the core-excited states in odd-mass Cu isotopes with the energies of excited 0^+ states in even-even Ni isotopes. Cu isotopes are more accessible experimentally than their Ni isotones, and we can learn more about shape coexistence in Ni from studying Cu. The $7/2^-$ states seem to follow the same parabola from ^{69}Cu to ^{79}Cu, indicating that both the 0^+ states in Ni and the $7/2^-$ states in Cu are based on intruder configurations. Similarly to how the 0^+ excited states in the Sn isotopic chain have a rotational band of 2^+, 4^+, 6^+ on top, the $9/2^-$ and $11/2^-$ states can be interpreted as

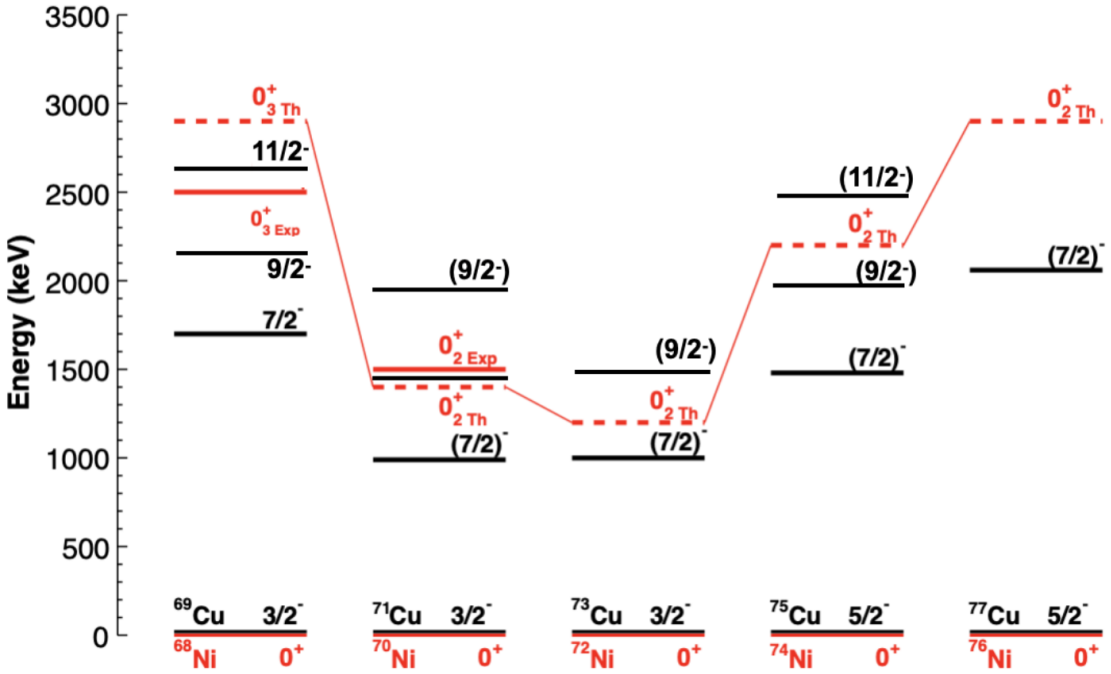

Figure 1.5: Systematics of 0^+ intruder states in even-even Ni isotopes and the corresponding intruder states in Cu. Figure from [14]. The Ni states are presented in red and Cu states are presented in black. Stippled lines are MCSM predictions, while filled lines are experimentally observed.

rotational excitations on top of the $7/2^-$ states in the odd-mass Cu isotopes. In order to completely confirm that these really are deformed bands, measuring the $B(E2)$ values is needed. However, the structure of the decay patterns and the parabola across the shell give strong indications that shape coexistence should also be expected for the Ni isotopes at the $Z = 28$ shell closure.

Chapter 2

Introduction to the papers

This thesis presents case studies of nuclear structure for neutron-rich nuclei, both far from stability and closer to the valley of stability. All nuclei studied are near or at closed shells, and the experimental results are compared to shell model calculations. While the first three papers present the structure of odd-odd nuclei ^{74,76,78}Cu, the fourth paper discusses the structure and shape coexistence in ^{126}Sn. In this way, this thesis includes both analysis of odd-odd nuclei only one proton away from magic numbers (Cu, $Z = 29$), and an even-even magic nucleus (Sn, $Z = 50$).

The data presented in these papers are from two different experimental campaigns. The Cu data were obtained in a large experimental campaign aimed at studying many nuclei in the ^{78}Ni region. The Sn data are from a separate experiment specifically designed for studying specific states in the nucleus of interest. The two experiments and main analysis methods are presented below, before the papers are included in their entireties following this chapter.

2.1 The Cu experiments

The data used for this analysis were gathered at two experiments performed in 2012 and 2013 at the RIKEN Nishina Center, Japan, as a part of the EURICA campaign [22, 23]. The EURICA campaign was a large collaborative effort between several institutes from different nations, where 12 Germanium Cluster detectors [24] from the EUROBALL collaboration [25], each consisting of seven individual HPGe detectors, were set up at the RIKEN facility [22]. The presented papers on ^{74,76,78}Cu are part of a long list of publications from these experiments, which aimed at measuring highly exotic nuclei in the ^{78}Ni region. The detector calibration and pre-sorting of the data was done by Zhengyu Xu, who is a co-author of all three Cu papers and the author of the PhD thesis [26] and paper [27] presenting the measurement of 20 previously unknown β-decay half-lives of neutron-rich nuclides in the region around ^{78}Ni from the same two experiments. The Oslo group was responsible for analysing the data on $^{74-77}$Cu, where ^{75,77}Cu were analysed by Frank Bello Garrote [12, 13]. The ^{78}Cu data were later obtained from Megumi Niikura, the main spokesperson of the experimental campaign, by request after

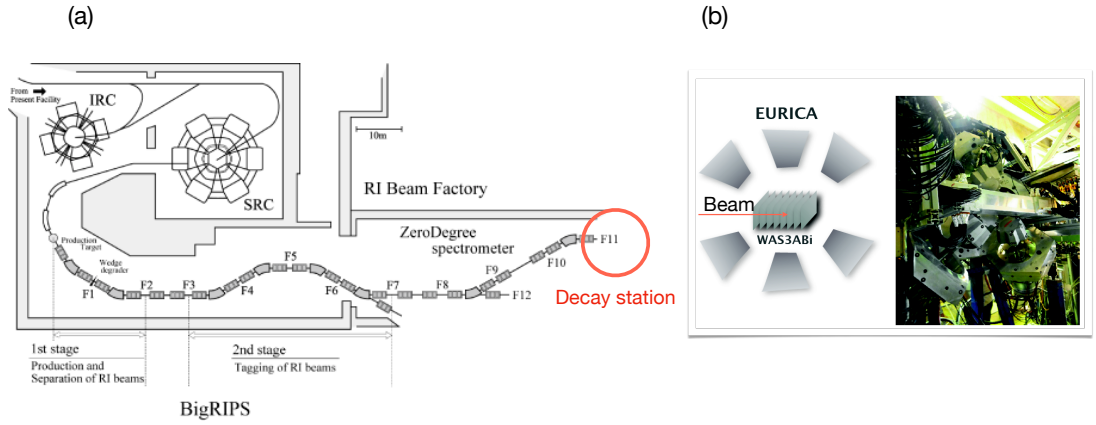

Figure 2.6: A schematic drawing of the RIKEN facility (a) [28], with a highlight of the decay station with EURICA and WAS3ABi, and a photo of the WAS3ABi detector (b).

$^{74-77}$Cu were analysed. An introduction to the experiment is presented in the following section.

For heavy nuclei, the most stable isotopes have increasingly larger neutron-to-proton ratios and fission of these heavy nuclei therefore results in fission fragments that are relatively neutron rich. Taking advantage of this, a fission reaction experiment was used to produce the neutron-rich exotic nuclei in the ^{78}Ni region. A beam of ^{238}U is accelerated by four ring cyclotrons up to 345 MeV/u and directed at a ^{9}Be target. The collision between the beam and target induces fission, and the fission fragments were identified in the BigRIPS fragment separator and the Zero-degree spectrometer. For an illustration of the facility, see Figure 2.6. In BigRIPS, the fission fragments were separated and identified based on their respective mass, atomic number, and charge. The separator was tuned to accept nuclei in the region of interest which then reach the decay stations at the end of the ZeroDegree spectrometer. The decay station was equipped with DSSSD silicon strip detectors (WAS3ABi) organised in eight layers for particle detection and the 12 HPGe EUROBALL detectors for γ detection. The highly pixelised WAS3ABi detected the implantation of ions and the subsequent electron emitted in β decay, and through time correlations the immediate γ rays following the β decays could be assigned to their nucleus of origin. Although the setup for the two experiments was mostly the same, slightly different tuning of BigRIPS was used. While the first experiment was tuned to optimise for ^{78}Ni, the second experiment was optimised for ^{81}Zn. Data from both experiments were used for the analysis of all three nuclei, but initial steps of the analysis had to be done for the two experiments separately and then later combined.

2.1.1 Analysis of the Cu data

Before the presented analysis of the Cu isotopes, no excited states were known for any of them. Level schemes are obtained by studying γ-γ coincidences, where data is sorted into coincidence matrices, i.e. two-dimensional energy histograms of γ rays that were detected within a prompt time window. Slicing the coincidence

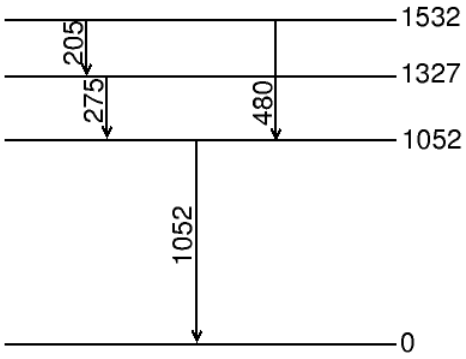

Figure 2.7: Partial level scheme for ^{76}Cu, showing four of the strongest transitions that together establish three excited states. States and γ transitions are marked by their energies in keV.

matrix at the energy of a specific transition, so-called gating, produces a one-dimensional spectrum of the coincident transitions. Investigating which γ-ray transitions are coincident and which are not allows constructing the level scheme. However, the time resolution for γ ray detection is not sufficient to tell in which order they were emitted. To place them in the correct order, one can either study their intensities or look at other transitions to determine the decay pattern. An example is shown in Figure 4 in Paper I. When gating on the 1052 keV peak in the γ-γ spectrum, several peaks are seen. One of them is the 480 keV peak. Gating on this one only returns the 1052 keV peak. This indicates that the 480 keV peak should be on top of the 1052 keV peak. Likewise, the 275 and 205 keV peaks are in mutual coincidence, but the 275 keV transition is more intense, which can only be explained if the transition receives feeding both from the 205 keV transition and from β decay directly. To compare transition intensities, one has to take the energy-dependent efficiency of the detectors into account. The two transitions of 275 keV and 205 keV are not in coincidence with the 480 keV transition, but the sum of them is 480 keV. This is a clear indication that they form a parallel cascade to the 480 keV transition. The corresponding level scheme is then drawn as shown in Figure 2.7 based on this γ-γ coincidence analysis example. The systematic analysis of coincidence relationships, energy sums and differences, and intensity arguments allowed constructing the final level schemes step by step.

The γ-ray intensities are not only important to build up the level scheme, but also to determine the β-decay feeding intensity into the excited states. Using the Radware gf3 software [29], the peaks are fitted for the two experiments separately using the single γ-ray spectra without any time restrictions. These fits give a curve with a corresponding centroid (energy) and area (counts), both with uncertainties from the fit, as illustrated in Figure 2.8. The energy of a peak is calculated as the mean of the two energies obtained from the two experiments. The γ-ray intensity is found by correcting the peak areas from the Radware fit for the detector efficiency, still separated into experiment one and two because the efficiency curves for the detectors were slightly different for the two experiments. The intensities from the two experiments are then summed to find the total intensity of the transition. This

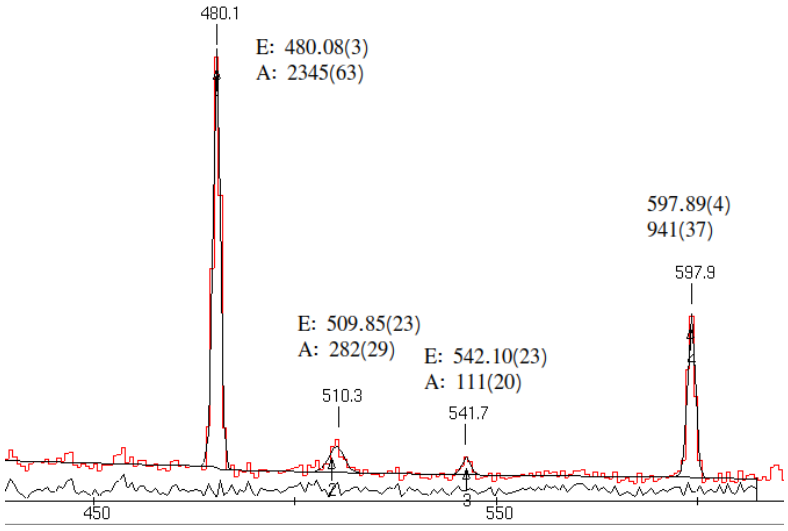

Figure 2.8: An example of the peak fitting. The black line is the fit of the red histogram containing the experimental energy histogram. The program finds and subtracts the background level and gives the area and energy of each peak as output. Energies are given in keV and areas are given in number of counts.

is divided by the number of ions detected[1] to give the absolute intensity. These are the intensities presented for each transition in the Cu papers.

The absolute intensities for the γ-ray transitions are used to calculate the β feeding to each state, which is a measure of how strongly the different states are directly populated in the β decay. The β feeding is calculated by summing the γ-ray intensities of transitions *from* a state, and subtracting the feeding *to* the state. An example is showed in Figure 2.9. The state X is fed directly by β decay and by two γ-ray transitions from higher-lying states, 400 keV with absolute intensity 7% and 250 keV with absolute intensity 5%. State X then decays by two γ-ray transitions, at 100 keV and 200 keV, with intensities 10% and 20%, respectively. The β feeding is then calculated as

$$\beta(X) = I(200) + I(100) - I(400) - I(250)$$

$$= 20\% + 10\% - 7\% - 5\% = 18\%$$

In addition to β-feeding to each state, another useful tool to describe the feeding to each state are $\log ft$ values [30]. These were obtained from the experimental intensities using the NNDC $\log ft$ calculator [31]. The strength of β-decay is classified into allowed transitions or transitions of various degrees of forbiddenness depending on the spin difference between the mother and daughter nucleus. These different decays have characteristic $\log ft$ values. For example, allowed Gamow-Teller 0^+ to 1^+ transitions typically have $4 < \log ft < 6$ [30]. Based on these values, it is possible to constrain spin values for the states in the β-decay daughter nucleus and in some cases also assign spin without measuring it directly. However, the $\log ft$ distributions for different spins overlap, as illustrated in Figure 2.10, and

[1]The method of finding the number of ions is described in Paper III.

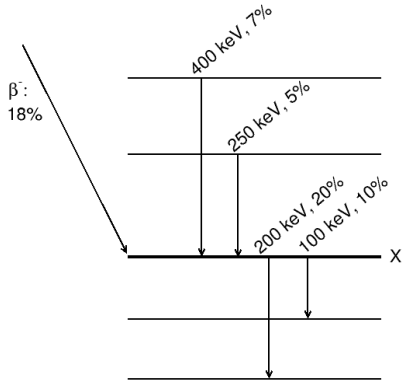

Figure 2.9: Illustration on how to calculate the β feeding to a given state, X.

can therefore not always be used for firm spin assignments, but rather to constrain possible spin values. A more direct way of measuring spin is presented in the context of the ^{126}Sn analysis.

In the articles, we present the logft values as lower limits and β-decay feeding as upper limits and argue that this is due to missing feeding and the so-called *Pandemonium effect* [32]. The Pandemonium effect appears in β-decay studies of highly unstable nuclei with high Q_β-values. For more stable nuclei with relatively low Q_β values, the total β-decay feeding is usually shared between observed states. For an exotic nucleus with a high Q_β-value, the β decay feeds several states in the daughter nucleus, including high-energy states. The following γ-ray transitions from these high-lying states might go unobserved due to the limited efficiency for high-energy γ rays in the detectors. In these cases, the β feeding to lower-lying states will mistakenly be larger than they in reality are, as the observed feeding to these states are the sum of the real β feeding and the unobserved γ feeding. An example is illustrated in Figure 2.11. Here, a hypothetical state at 2 MeV receives 10% of the β feeding, while the state at 6 MeV receives 4% of the feeding. However, the state at 6 MeV goes unobserved in the experiment due to low statistics for the high-energy γ rays. As only the γ decay from (and not *to*) the 2 MeV state is observed, the feeding to the 2 MeV state is erroneously observed as 14%, instead of 10%. Consequently, the logft-value will be calculated as if the state receives 14% feeding, and the logft will be lower than the correct value.

2.2 The Sn experiment

The ^{126}Sn data are obtained from an experiment carried out at the Tandem Laboratory of the Horia Hulubei National Institute for Physics and Nuclear Engineering (IFIN-HH), Romania, during the autumn of 2019. The main objective of this experiment was to find evidence for excited 0^+ state(s) to be able to continue the systematics of the isotopic chain, where excited 0^+ states are observed for the even-even isotopes between $A = 110$ and $A = 124$. For the excited 0^+ states near neutron mid-shell around ^{116}Sn there is strong evidence that they are built on deformed intruder configurations with particle-hole excitations across the $Z = 50$

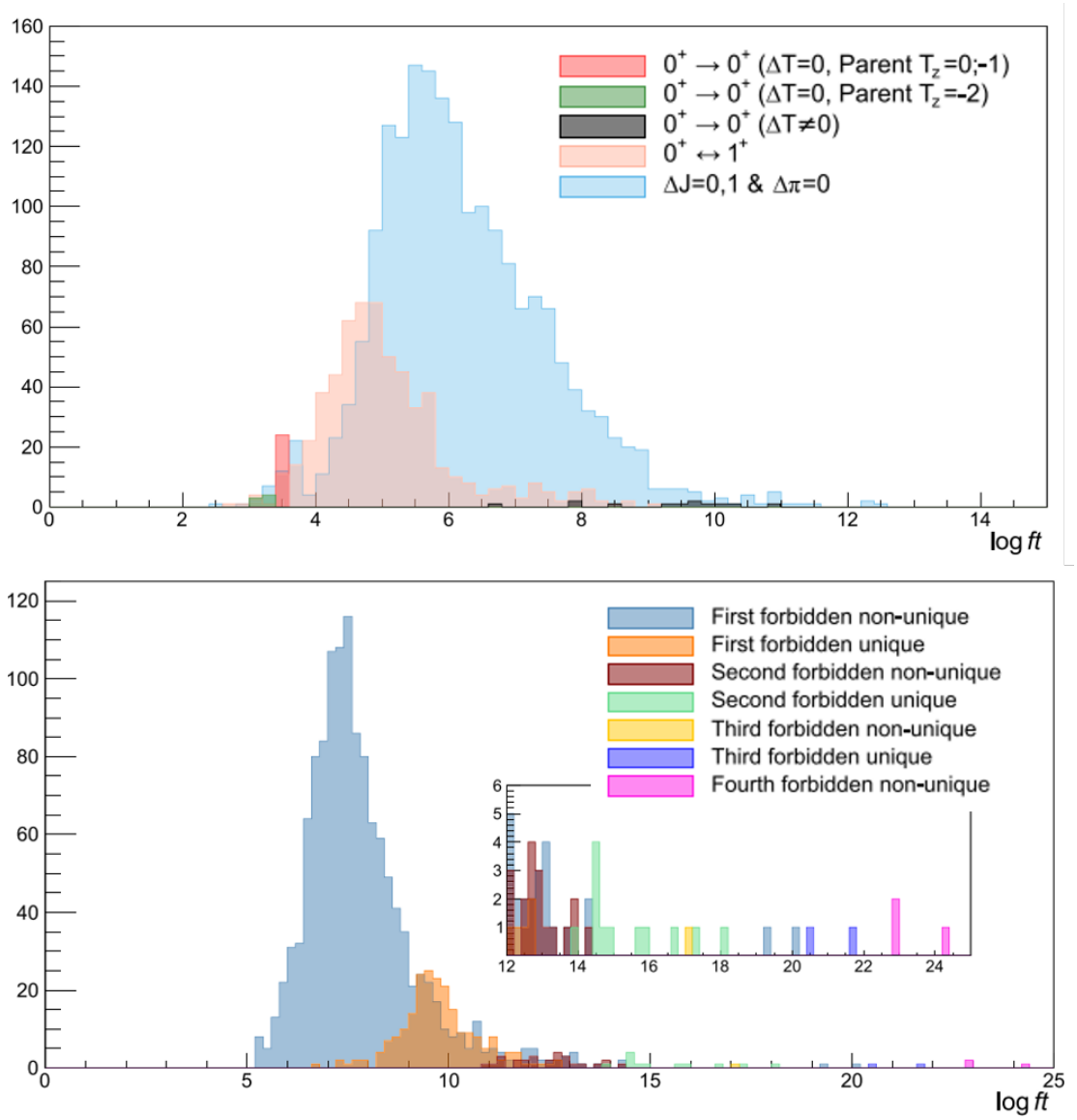

Figure 2.10: Figure adapted from [30] showing the log ft-values for different degrees of forbiddenness, illustrating the overlap between them.

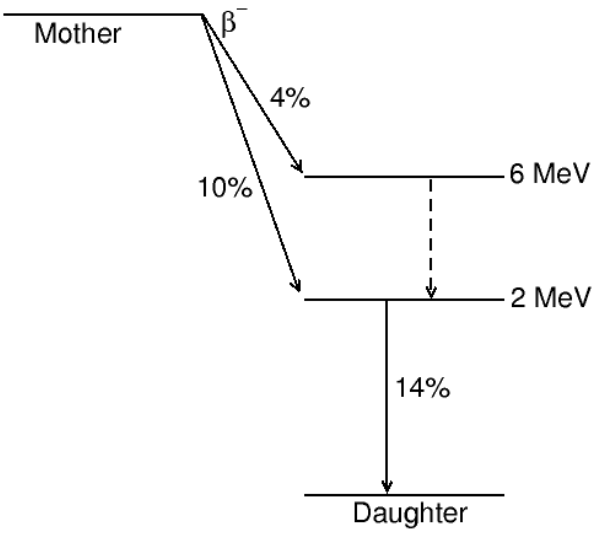

Figure 2.11: Illustration of missing feeding. In reality, the mother nucleus feeds both the 2 and 6 MeV states. However, only the state at 2 MeV and its decay are observed. Because the β-feeding to each state is not measured directly but calculated based on outgoing and incoming γ rays, the β-feeding to the state at 2 MeV is mistakenly measured as 14%.

shell closure [33]. The experiment on ^{126}Sn had the goal to learn more about the nature of excited 0^+ states by extending their systematics towards heavier isotopes. Previous studies of ^{126}Sn provided information about excited states through the β decay of ^{126}In [34], similar to the way the Cu isotopes are studied in this thesis. However, β-decay from ^{126}In to ^{126}Sn originates from the $3^{(+)}$ ground state or the (8^-) isomeric state. With β-decay from higher spin-states, it is much less likely to populate 0^+ states.

As the 0^+ excited state(s) were the main motivation to study ^{126}Sn, the experimental method was chosen specifically for its ability to populate excited 0^+ states. The ideal reaction to study deformed 0^+ states based on two-particle-two-hole excitations in ^{126}Sn would be the two-proton transfer reaction on ^{124}Cd, e.g. ^{124}Cd(^{3}He,n)^{126}Sn. This would require a radioactive ^{124}Cd beam, a ^{3}He target, and the detection of neutrons, all of which are experimental challenges. On the other hand, two-neutron transfer reactions have been shown to populate excited 0^+ states, including deformed intruder states, although with lower cross section [33, 35].

The ^{126}Sn experiment was inspired by a similar experiment using the two-neutron transfer reaction at IFIN-HH to populate excited 0^+ states in ^{66}Ni, showing evidence for three previously unobserved 0^+ states [35]. An ^{18}O beam was accelerated by the 9 MV Tandem accelerator to 56 MeV, slightly below the Coulomb barrier, and directed at a ^{124}Sn target. As the ^{18}O beam contains two excess neutrons outside a doubly magic core, this projectile has a relatively high probability of transferring a neutron pair in a nuclear reaction. However, other possible reactions using the same beam and target also have high cross sections

and the data shows high amounts of both fusion evaporation reactions and α transfer reactions. The ^{124}Sn target was mounted in the HPGe array ROSPHERE [36] for γ-ray detection, using the SORCERER [37] particle detector to detect ejected fragments after the collision. By applying energy and time conditions on the events detected with SORCERER and allowing only γ-ray events detected in coincidence with this, the γ ray spectra could be greatly cleaned by suppressing fusion evaporation channels, and to some extent also α transfer reactions.

2.3 Analysis of the ^{126}Sn data

As ^{126}Sn is less exotic than the ^{74,76,78}Cu isotopes, a partial level scheme of ^{126}Sn was already known from previous experiments with the first spectroscopy studies being performed as early as the 1970s [34]. This is the first time that a two-neutron transfer reaction is used in combination with high-resolution γ-ray spectroscopy.

The first step of the analysis was to expand the level scheme and look for new excited states. This is done using γ-γ coincidence relations, similar to the analysis of the Cu isotopes. Most importantly, we were looking for 0^+ candidates, likely to be populated directly in the reaction and then decay to the 2^+ excited states. Other new states are also of interest even if they are not 0^+ candidates, and a thorough γ-γ coincidence analysis was performed to look for those. After establishing the expanded level scheme and finding 0^+ candidates, the next step was to study the spins to firmly assign possible 0^+ states.

In theory, if the orientation of a nucleus is known, it is possible to measure the angular distribution of the emitted γ rays with respect to the spin orientation of the nucleus, which provides information on the multipolarity of the γ-ray transition. If the spin of either the initial or final state is known, the multipolarity of the transition constrains the spin of the other state. However, the orientation of a nucleus is usually unknown and indirect methods must be applied in order to utilise angular distributions. One method is to measure the relative angles between two γ-ray emissions in a cascade. The detection of the first γ ray at a specific angle puts constraints on the spin orientation of the nucleus in the intermediate state, and the angular distribution of the second transition is then measured with respect to this anisotropic spin orientation. Using a setup with γ-ray detectors covering a large range of angles, it is possible to determine the angular correlation as a function of relative emission angles and compare this with theoretical functions for different spin sequences.

The angular distribution of γ-ray emission is given by the difference between spin I_i of the initial state and spin I_f of the final state. When looking at subsequent γ transitions in a cascade, their angular correlation is given by the function

$$W(\theta) = 1 + A_2 P_2(\cos\theta) + A_4 P_4(\cos\theta), \tag{2.1}$$

where the $P_n(\cos\theta)$ are Legendre polynomials, and A_2 and A_4 are angular correlation coefficients that depend on the spins, multipolarities, and mixing angles of the states and transitions in the cascade. The theoretical angular correlation

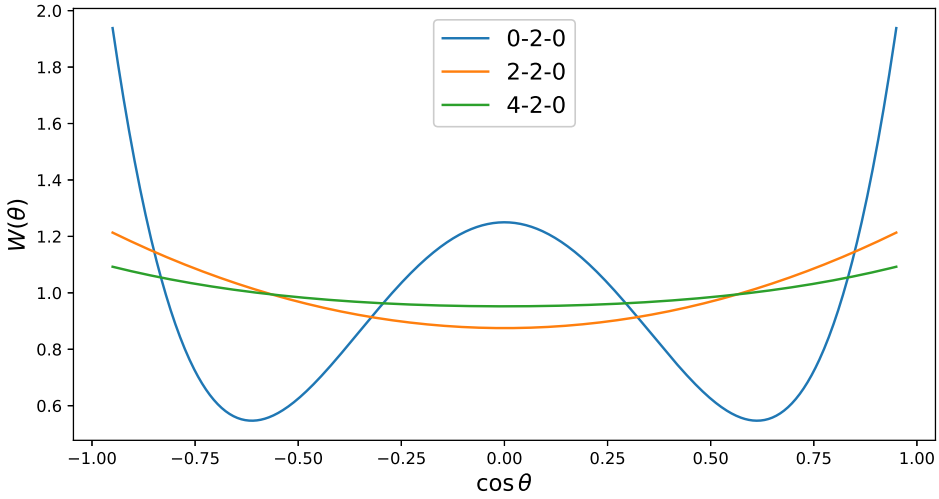

Figure 2.12: Theoretical distribution of angles between two γ rays in a cascade for different spin transitions assuming pure multipolarities with no mixing.

coefficients, which can be calculated or found in Tables [38] have to be corrected for the finite opening angles of the detectors.

This method could be used to obtain the spin of the newly observed states in ^{126}Sn. In practice, the theoretical angular distribution between two γ rays is plotted for several possible spin assignments and compared with the experimental data. A plot of the theoretical angular correlation for cascades with various spin sequences is shown in Figure 2.12.

To perform the angular correlation analysis, the angle between each individual detector pair was used. With 25 HPGe detectors the total number of detector pairs is $25 \times 24/2 = 300$. Detector pairs of similar relative angles are grouped together to increase statistics for each data point. Exploiting the fact that the angular distributions for different spin transitions are symmetric about 90 degrees (see Figure 2.12), the angles above 90 degrees are instead grouped with their counterpoint below 90 degrees, giving more data points to each angle under study. The different groups are presented in Table 2.1.

Because the groups have different numbers of detector pairs, and thus also much variation in the amount of statistics, the number of events have to be normalised. An example case is presented in Figure 2.13, showing two transitions decaying to the first excited 2^+ state, which further decays to the 0^+ ground state. The 909 keV transition decays from a known 4^+ state, and the 1068 keV decays from a state with unknown spin. It is the spin of this state that we are trying to measure. In order to perform the analysis we need both significant statistics in the 1068 keV and the 1141 keV transition in coincidence *and* another transition (909 keV) feeding into the 1141 keV state from an excited state of known spin. The γ-ray coincidences are sorted into γ-γ matrices depending on the relative angle between the detector pair that detected the event. For each angle group, we gate on the 1141 keV transition in the γ-γ matrix and measure the area of the 909 and 1068 keV transitions. The area of the 1068 keV transition is then normalised to the

Table 2.1: Table presenting the eight groups of detector angles giving one data point each. In each group, there are slightly different angles between the detector pairs, which are presented in the second column. The two columns to the right present the number of detector pairs per angle and the total number of detector pairs per group.

Group	**Angles in group**	**# detector pairs**	**# in group**
21	20	20	40
	21	20	
34	33	20	50
	34	20	
	36	10	
42	40	10	110
	41	60	
	43	40	
53	53	40	40
60	58	20	100
	61	40	
	63	40	
70	67	20	50
	70	20	
	72	10	
73	73	60	70
	74	10	
81	79	80	140
	81	20	
	84	40	

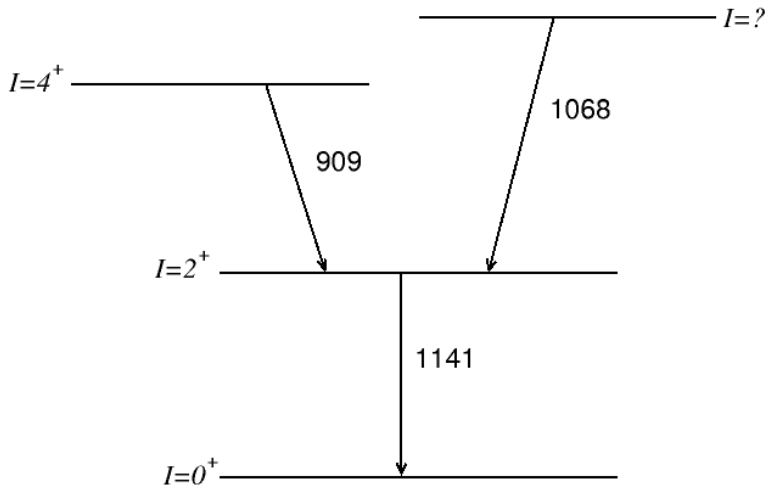

Figure 2.13: An example level scheme, showing a 1068 keV transition decaying from a state with unknown spin. In order to properly normalise the data, the intensity of all three transitions needs to be measured.

Table 2.2: Theoretical angular correlation coefficients A_2 and A_4 for selected spin sequences [38, 39], assuming pure multipolarities with no mixing.

	0-2-0	**1-2-0**	**2-2-0**	**3-2-0**	**4-2-0**	**5-2-0**
A_2	0.357142	-0.25	0.249999	-0.0714286	0.102041	0.178571
A_4	1.142857	0	0	0	0.00907129	-0.00432900

area of the 909 keV transition, taking the angular correlation of the 4-2-0 cascade into account, as described in Paper IV. Normalising in this way by a transition of known multipolarity eliminates the dependence of the angular correlation on the detector efficiencies and opening angles. The normalised angular correlation angular correlation data can then be directly compared with theoretical angular correlation functions for different hypotheses for the unknown spin of the initial state.

Part II

The papers

Paper I

Evolution of the nuclear structure in neutron-rich Cu isotopes: First spectroscopy of odd-odd ^{74}Cu and ^{76}Cu

Under review for publishing in PRC

I

Paper II

First spectroscopic study of odd-odd ^{78}Cu

Phys. Rev. C 107, 044301 (2023)

II

II

First spectroscopic study of odd-odd ^{78}Cu

L. G. Pedersen,[1,*] E. Sahin,[1,†] A. Görgen,[1] F. L. Bello Garrote,[1] Y. Tsunoda,[2] T. Otsuka,[3] M. Niikura,[3] S. Nishimura,[4] Z. Xu,[3,5] H. Baba,[4] G. Benzoni,[6] F. Browne,[4,7] A. M. Bruce,[7] S. Ceruti,[6] F. C. L. Crespi,[6,8] R. Daido,[9,4] G. de Angelis,[10] M.-C. Delattre,[11] Zs. Dombradi,[12] P. Doornenbal,[4] Y. Fang,[9,4] S. Franchoo,[11] G. Gey,[4,13] A. Gottardo,[14] T. Isobe,[4] P. R. John,[15] H. S. Jung,[16] I. Kojouharov,[17] T. Kubo,[4] N. Kurz,[17] I. Kuti,[12] Z. Li,[18] G. Lorusso,[4] I. Matea,[11] K. Matsui,[3] D. Mengoni,[15] T. Miyazaki,[3] V. Modamio,[1] S. Momiyama,[3] A. I. Morales,[6,8,19] P. Morfouace,[11] D. R. Napoli,[20] F. Naqvi,[21] H. Nishibata,[9] A. Odahara,[9] R. Orlandi,[22,23] Z. Patel,[4,24] S. Rice,[4,24] H. Sakurai,[3,4] H. Schaffner,[17] L. Sinclair,[4,25] P.-A. Söderström,[4,26] D. Sohler,[12] I. G. Stefan,[11] T. Sumikama,[27] D. Suzuki,[11] R. Taniuchi,[3,25] J. Taprogge,[4,28] Z. Vajta,[4,12] J. J. Valiente-Dobón,[14] H. Watanabe,[29] V. Werner,[21,30] J. Wu,[4,18] A. Yagi,[9,4] M. Yalcinkaya,[31] R. Yokoyama,[2] and K. Yoshinaga[32]

[1]*Department of Physics, University of Oslo, NO-0316 Oslo, Norway*
[2]*Center for Nuclear Study, The University of Tokyo, 7-3-1 Hongo, Bunkyo-ku, Tokyo 113-0033, Japan*
[3]*Department of Physics, the University of Tokyo, Hongo 7-3-1, Bunkyo-ku, 113-0033 Tokyo, Japan*
[4]*RIKEN Nishina Center, 2-1 Hirosawa, Wako, Saitama 351-0198, Japan*
[5]*University of Hong Kong, Hong Kong, China*
[6]*Istituto Nazionale di Fisica Nucleare, Sezione di Milano, Via Celoria 16, I-20133 Milano, Italy*
[7]*School of Computing, Engineering and Mathematics, University of Brighton, Brighton, BN2 4GJ, United Kingdom*
[8]*Dipartimento di Fisica dell'Università degli Studi di Milano, Via Celoria 16, I-20133 Milano, Italy*
[9]*Department of Physics, Osaka University, 1-1 Machikaneyama, Toyonaka, Osaka 560-0043, Japan*
[10]*INFN Laboratori Nazionali di Legnaro, Legnaro (Pd), 35020 Legnaro, Italy*
[11]*Institut de Physique Nucleaire (IPN), IN2P3-CNRS, Universite Paris-Sud 11, F-91406 Orsay Cedex, France*
[12]*Institute for Nuclear Research (Atomki), Debrecen H-4001, Hungary*
[13]*LPSC, Universite Joseph Fourier, CNRS/IN2P3, Institut National Polytechnique de Grenoble, 38026 Grenoble Cedex, France*
[14]*Istituto Nazionale di Fisica Nucleare, Laboratori Nazionali di Legnaro, I-35020 Legnaro, Italy*
[15]*INFN Sezione di Padova and Dipartimento di Fisica, Università di Padova, 35131 Padova, Italy*
[16]*Department of Physics, University of Notre Dame, Notre Dame, Indiana 46556, USA*
[17]*GSI Helmholtzzentrum für Schwerionenforschung GmbH, D-64291 Darmstadt, Germany*
[18]*Department of Physics, Peking University, Beijing 100871, China*
[19]*IFIC, CSIC-Universitat de València, E-46071 València, Spain*
[20]*INFN Laboratori Nazionale di Leganro, Padova, I-35020 Legnaro, Italy*
[21]*Wright Nuclear Structure Laboratory, Yale University, New Haven, Connecticut 06520-8120, USA*
[22]*Instituut voor Kern- en StralingsFysica, K.U. Leuven, B-3001 Heverlee, Belgium*
[23]*Advanced Science Research Center, JAEA, Tokai, Ibaraki 319-1195, Japan*
[24]*Department of Physics, University of Surrey, Guildford GU2 7XH, United Kingdom*
[25]*Department of Physics, University of York, Heslington, York YO10 5DD, United Kingdom*
[26]*Extreme Light Infrastructure-Nuclear Physics (ELI-NP)/Horia Hulubei National Institute for Physics and Nuclear Engineering (IFIN-HH), Str. Reactorului 30, Bucharest-Măgurele 077125, Romania*
[27]*Department of Physics, Tohoku University, 6-3 Aramaki-Aoba, Aoba, Sendai 980-8578, Japan*
[28]*Instituto de Estructura de la Materia, CSIC, E-28006 Madrid, Spain*
[29]*International Research Center for Nuclei and Particles in the Cosmos, Beihang University, Beijing 100191, China*
[30]*Institut für Kernphysik, Technische Universität Darmstadt, Schlossgartenstr. 9, 64289 Darmstadt, Germany*
[31]*Department of Physics, Faculty of Science, Istanbul University, Vezneciler/Fatih, 34134, Istanbul, Turkey*
[32]*Department of Physics, Tokyo University of Science, 2641 Yamazaki, Noda, Chiba 278-8510, Japan*

(Received 6 October 2022; revised 3 January 2023; accepted 9 January 2023; published 3 April 2023)

Nuclei in the vicinity of ^{78}Ni are important benchmarks for nuclear structure, which can reveal changes in the shell structure far from stability. Spectroscopy of the odd-odd isotope ^{78}Cu was performed for the first time in an experiment with the EURICA setup at the Radioactive Isotope Beam Factory at RIKEN Nishina Center. Excited states in the neutron-rich isotope were populated following the β decay of ^{78}Ni produced by in-flight fission and

*l.g.pedersen@fys.uio.no
†eda.sahin@fys.uio.no

separated by the BigRIPS separator. A level scheme based on the analysis of γ-γ coincidences is presented. Tentative spin and parity assignments were made when possible based on the β-decay feeding intensities and γ-decay properties of the excited states. Time correlations between β and γ decay show clear indications of an isomeric state with a half-life of 3.8(4) ms. Large-scale Monte Carlo shell-model calculations were performed using the A3DA-m interaction and a valence space comprising the full fp shell and the $1g_{9/2}$ and $2d_{5/2}$ orbitals for both protons and neutrons. The comparison of the experimental results with the shell-model calculations allows interpreting the excited states in terms of spin multiplets arising from the proton-neutron interaction. The results provide further insight into the evolution of the proton single-particle orbitals as a function of neutron number, and quantitative information about the proton-neutron interaction outside the doubly magic ^{78}Ni core.

DOI: 10.1103/PhysRevC.107.044301

I. INTRODUCTION

One of the fundamental questions in nuclear physics is how nuclear structure changes when moving away from well-known stable nuclei towards exotic nuclei with large proton-neutron asymmetry. Doubly magic nuclei and their neighbors play a crucial role for understanding the mechanisms that affect the energies and ordering of single-particle orbitals and the size of shell gaps [1,2]. The nucleus ^{78}Ni is of particular interest for studies of shell evolution. With 28 protons and 50 neutrons, it has the largest neutron-to-proton ratio of all closed-shell nuclei with traditional magic numbers. The doubly magic character of ^{78}Ni was recently confirmed in a spectroscopic study that identified the first excited 2^+ state at a high excitation energy of 2.6 MeV [3]. Robust shell closures for both $Z = 28$ and $N = 50$ are consistent with β-decay half-lives of nuclei in the region [4] and with the masses of neutron-rich Cu isotopes [5]. Nuclei with few valence particles or holes outside a ^{78}Ni core represent therefore important benchmarks for theoretical models. The nucleus ^{78}Cu with $Z = 29$ and $N = 49$ is ideally suited to obtain information about the proton-neutron interaction outside the ^{78}Ni core. Properties of nuclei in the vicinity of ^{78}Ni, in particular masses and β-decay half-lives but also the occurrence of isomeric states, are furthermore important for modeling the nucleosynthesis in the region of the first r-process abundance peak [6,7].

Earlier experiments in the ^{78}Ni region have seen evidence for an inversion of the proton $\pi 2p_{3/2}$ and $\pi 1f_{5/2}$ orbitals [8,9]. The ordering of the two states becomes inverted in ^{75}Cu, where the ground state was found to have $I^\pi = 5/2^-$ [8], and an isomeric $3/2^-$ state was found at very low excitation energy [10]. The excitation energy of the $3/2^-$ state continues to increase relative to the $5/2^-$ ground state in ^{77}Cu [9] and ^{79}Cu [11], consistent with the crossing of the $\pi 1f_{5/2}$ and $\pi 2p_{3/2}$ orbitals. The change in single-particle energies was explained by the monopole component of the tensor interaction, which is attractive between the $\nu 1g_{9/2}$ and $\pi 1f_{5/2}$ orbitals but repulsive between the $\nu 1g_{9/2}$ and $\pi 2p_{3/2}$ orbitals [12]. In ^{78}Cu, with only one proton and one neutron hole outside the doubly magic core, relatively pure configurations are expected. The ground state and excited states at low excitation energy are expected to be dominated by the negative-parity multiplet arising from the coupling of an odd proton in the $\pi 1f_{5/2}$ orbital with a neutron hole in the $\nu 1g_{9/2}$ orbital.

The easiest way to couple the valence particles to positive-parity states is by neutron excitation from the $\nu 2p_{1/2}$ into the $\nu 1g_{9/2}$ orbital, leaving an unpaired neutron in the $\nu 2p_{1/2}$ orbital. Positive-parity states are expected to be found at higher excitation energy, and those with low spin are expected to be strongly fed in β decay by allowed transitions.

Shell-model calculations for the heavy odd-odd Cu isotopes were performed earlier by Van Roosbroeck *et al.* using schematic δ and quadrupole-quadrupole (QQ) interactions for single proton and neutron shells outside a ^{68}Ni core, as well as using a larger valence space comprising the pf and $1g_{9/2}$ orbitals for both protons and neutrons with a more realistic interaction [13]. The results of the calculations reflected the transition from particle-particle to particle-hole coupling as neutrons fill the $\nu 1g_{9/2}$ orbital, consistent with expectations from the parabolic rule [14].

Monte Carlo shell-model (MCSM) calculations [15] based on a larger valence space outside a ^{40}Ca core with the A3DA-m interaction [16] were able to reproduce detailed spectroscopic data for both ^{77}Cu [9] and ^{79}Cu [11]. Extending the experimental spectroscopic information to heavier odd-odd Cu isotopes is crucial for understanding the interaction between proton particles and neutron holes outside the ^{78}Ni core and to provide additional benchmarks for the MCSM calculations. It was furthermore shown that residual proton-neutron interactions between the pf and sdg shells have implications for calculating electron-capture rates during core collapse supernovae [17].

Before the present experiment, no excited states in ^{78}Cu were known. Its half-life has previously been measured to be 330.7 ± 2.0 ms [4]. Magnetic-dipole and electric-quadrupole moments have been measured for the ground states up to $A = 78$ [18], which found a tentative assignment of (6^-) for ^{78}Cu. The present work provides the first spectroscopic information on the odd-odd isotope ^{78}Cu. Experimental details and the data analysis are described in Secs. II and III, respectively. Results including spectra, level schemes, and spin-parity assignments, are presented in Sec. IV. The results are discussed and compared with MCSM calculations in Sec. V, followed by a summary and conclusions in Sec. VI.

II. EXPERIMENTAL SETUP

The data presented in this article were obtained in experiments carried out at the Radioactive Isotope Beam Factory (RIBF) of the RIKEN Nishina Centre for Accelerator-based Science outside Tokyo, Japan, during two separate beam times as part of the EURICA campaign [19]. A primary beam of

^{238}U was accelerated subsequently by four cyclotrons to an energy of 345 MeV per nucleon with an average intensity of 10 pnA. In-flight fission reactions of the incident ^{238}U projectiles were induced on a ^{9}Be target of 555 mg/cm^2 areal density, which was located at the F0 focal point at the entrance of the BigRIPS fragment separator [20]. The fission fragments were separated in the first stage of the BigRIPS separator by using the $B\rho$-ΔE-$B\rho$ method [21]. Particle identification (PID) was performed in the second stage of the fragment separator by combining information on the time-of-flight through the separator with the magnetic rigidity $B\rho$ and the characteristic energy loss ΔE of the fragments. The ions of interest were further transmitted through the ZeroDegree spectrometer [21] to the focal point F11, where their β decay and subsequent γ-ray emission were detected. A resulting PID plot can be found in Ref. [4]. The settings of the BigRIPS separator were optimized for the transmission of ^{78}Ni and ^{81}Zn, respectively, during the two experiments.

The separated fission fragments were implanted into the wide-range active silicon-strip stopper array for beta and ion detection (WAS3ABi) [22], which consisted of a stack of eight double-sided silicon strip detectors (DSSSDs). Each detector had 60 horizontal and 40 vertical strips of 1 mm pitch, resulting in a total of 2400 pixels of size 1×1 mm^2 per detector. Each detector had a thickness of 1 mm, with 0.5 mm separation in depth between the detectors. To ensure that the ions were stopped in the center of WAS3ABi, a thin Al degrader was located in front of the detectors. The WAS3ABi array was surrounded by the EURICA array of 12 Euroball Cluster detectors. Each Cluster detector consisted of seven HPGe detectors, yielding a total of 84 Ge crystals with an absolute photopeak efficiency of $\approx$6.5% for 1.3 MeV γ rays. Ion implantation, β decay, and γ decay events were recorded in time-stamped list mode, allowing the correlation of γ-decay events with the β decays of specific fission fragments that were identified in mass and atomic number. More details on the experimental setup can be found in Refs. [19,22].

III. DATA ANALYSIS

As a first step, subsets of data were generated according to the atomic number Z and mass number A of the ions that were identified in BigRIPS and implanted into WAS3ABi. Ion implantation events were correlated in time and position with subsequent β decays. A total of 7.2×10^3 ^{78}Ni ions were implanted, and 3.0×10^3 correlated β-decay events were detected. The β-decay half-life of ^{78}Ni was found to be $T_{1/2} = 122.2(51)$ ms in a separate analysis of the same data [4], while the Q_β value is 9910 (400) keV [23]. Finally, γ rays detected in the Ge detectors were correlated in time with β-decay events in the Si detectors. The data from the two experiments were analyzed separately, and the resulting γ-ray spectra and γ-γ coincidence matrices were combined afterwards. The individual steps of the data analysis are described in more detail in the following.

Signals from heavy-ion implantation in the DSSSDs are easily distinguished from the detection of β-decay electrons by their signal amplitude. For each implantation event of a ^{78}Ni ion, the data were scanned for the subsequent β decays within a given time window of 2 s. If more than one β-decay event were registered within the correlation time window, only the first one was considered. To reduce the number of random coincidences between implantation and β-decay events, it was required that the implanted ion and β-decay electron were detected in the same, a neighboring, or next to neighboring pixel of the same DSSSD layer.

Finally, correlated events between implanted ions and β decays were used to select γ rays that were promptly following the β decay of ^{78}Ni, within a time window of approximately 200 ns. The information on the time difference between β decays and detected γ rays was furthermore used to search for isomeric decays. In the case that two neighboring crystals within the same Ge cluster detector gave coincident signals, their energies were summed to account for Compton scattering and to increase the detection efficiency for γ rays with high energy.

γ-ray singles spectra were sorted for different correlation time windows between the ion implantation and β-decay events. Because the detection efficiency for electrons in the DSSSD is less than 100%, the β decay can remain undetected. In case a subsequent β decay (or β-delayed neutron decay) occurs within the correlation time window, γ rays from the decay daughter or even granddaughter can appear in the spectrum. Limiting the correlation time to short intervals of the order of the half-life of ^{78}Ni strongly suppresses γ rays originating from subsequent decays but also removes γ rays occurring within ^{78}Cu. The relative suppression of γ rays as a function of correlation time was used to assign unknown γ rays to ^{78}Cu. Known γ rays following the decay of ^{78}Cu into ^{78}Zn, [13] were used to validate the procedure. After the assignment of the strongest γ rays to ^{78}Cu, the strict time constraint between implantation and β decay was relaxed to search for γ-γ coincidences and to construct the level scheme in a compromise between high statistics for the γ rays of interest and suppressing γ rays from daughter decays.

Figure 1 shows a γ-ray singles spectrum for ^{78}Cu. To maximize the level of statistics, a relatively long correlation time window of 2 s was used, resulting in stronger contributions from the daughter decays in ^{77,78}Zn. All peaks that are labeled by their energy were assigned to ^{78}Cu. Some transitions, however, could not be placed in the level scheme because of lacking γ-γ coincidence relationships. These transitions, which are labeled by their energies in parentheses, were assigned to ^{78}Cu based only on their time correlation with the β-decay detection. Where possible, coincidence relationships between γ rays were used to validate their assignment to ^{78}Cu. Examples for gated coincidence spectra are shown in Fig. 2. Only γ rays that could be placed unambiguously were included in the level scheme.

The absolute intensity of β-decay feeding was determined from the intensity balance of γ rays feeding and depopulating a given state, which was corrected for detection efficiency and internal conversion and normalized to the number of implanted ions. However, because of the incomplete level scheme and missing γ-ray feeding from above, this apparent β feeding is only a limit, and a conversion into logft values is not meaningful. The probability for β-delayed neutron emission was measured to be $P_n = 25.8(38)\%$ [24]. The observed

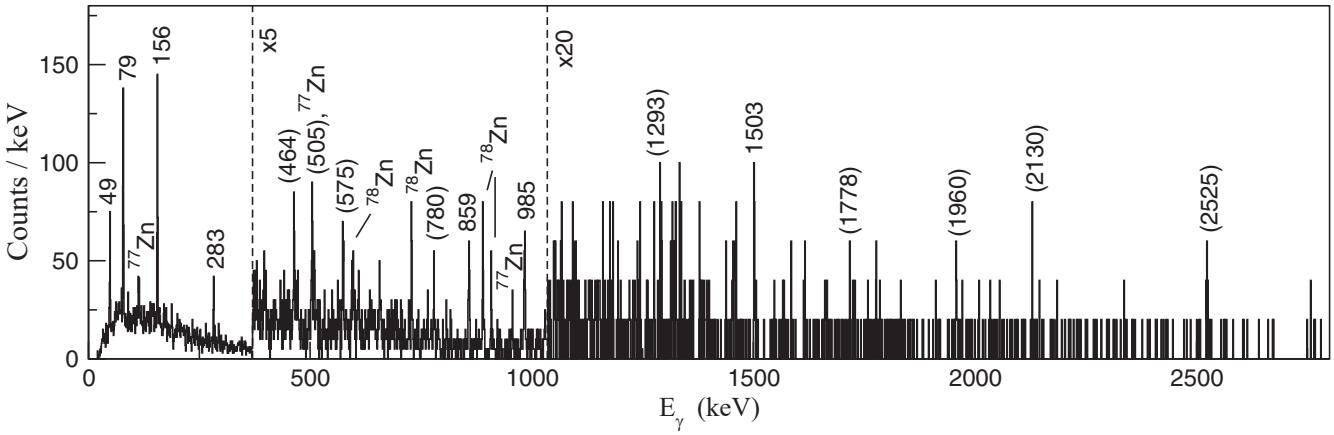

FIG. 1. γ-ray singles spectrum for ^{78}Cu. Note that the higher-energy regions of the spectrum were scaled by the indicated factors. An ion-β correlation window of 2 s was used. Peaks marked by their energy (in keV) are transitions assigned to ^{78}Cu. Energies are given in parentheses for transitions that were assigned to ^{78}Cu but could not be placed in the level scheme. Transitions following the subsequent β and β-n decay of ^{78}Cu are labeled as ^{78}Zn and ^{77}Zn, respectively. The 505 keV transition appears in both ^{78}Cu and the β-n daughter ^{77}Zn.

apparent β feeding accounts for less than 58% of the decays of implanted ions. Taking into account P_n, less than 78% of β-decay feeding was observed. The values for the total observed feeding represents only upper limits and a significant fraction of feeding strength could therefore remain unobserved.

IV. RESULTS

The decay scheme for ^{78}Cu is shown in Fig. 3. The information presented in the decay scheme is furthermore summarized in Table I, together with information on γ-ray intensities and uncertainties for all quantities. It should be noted that no excited states were known prior to the present experiment. The analysis of time correlations allowed associating 16γ-ray transitions with ^{78}Cu, as indicated in Fig. 1. Of these, seven could be placed in the decay scheme based on their coincidence relationships.

The ground-state spin of ^{78}Cu was previously assigned as $(4, 5)^-$ [13] based on the feeding of states in the β-decay daughter ^{78}Zn, and, in later works, as (6^-) [25] and (5^-) [26]. A laser spectroscopy experiment showed best agreement with $I = 6$, suggesting a ground-state spin-parity of (6^-) [18].

The three strongest transitions, with energies of 49, 79, and 156 keV are in mutual coincidence, as shown in Fig. 2. Because they are much stronger than any other transition, it is reasonable to assume that they form a cascade built on the ground state. It can be furthermore assumed that the low-energy transitions connect members of the negative-parity $\pi 1f_{5/2} \times \nu 1g_{9/2}^{-1}$ multiplet, because other configurations are only expected at higher excitation energy. The intensities

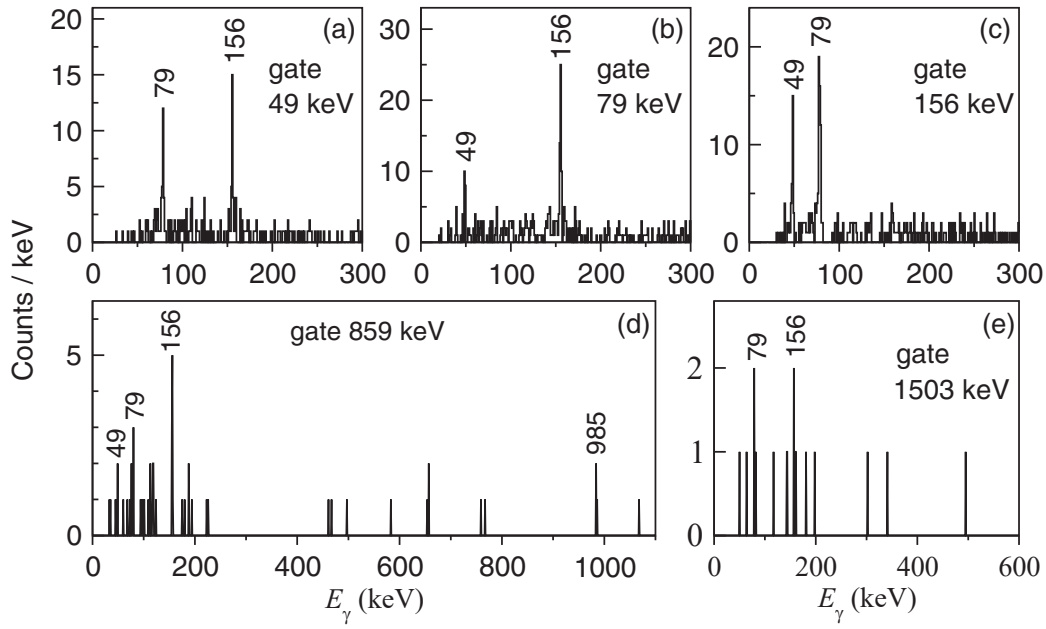

FIG. 2. γ-γ coincidence spectra for ^{78}Cu gated on the (a) 49 keV, (b) 79 keV, (c) 156 keV, (d) 859 keV, and (e) 1503 keV transition.

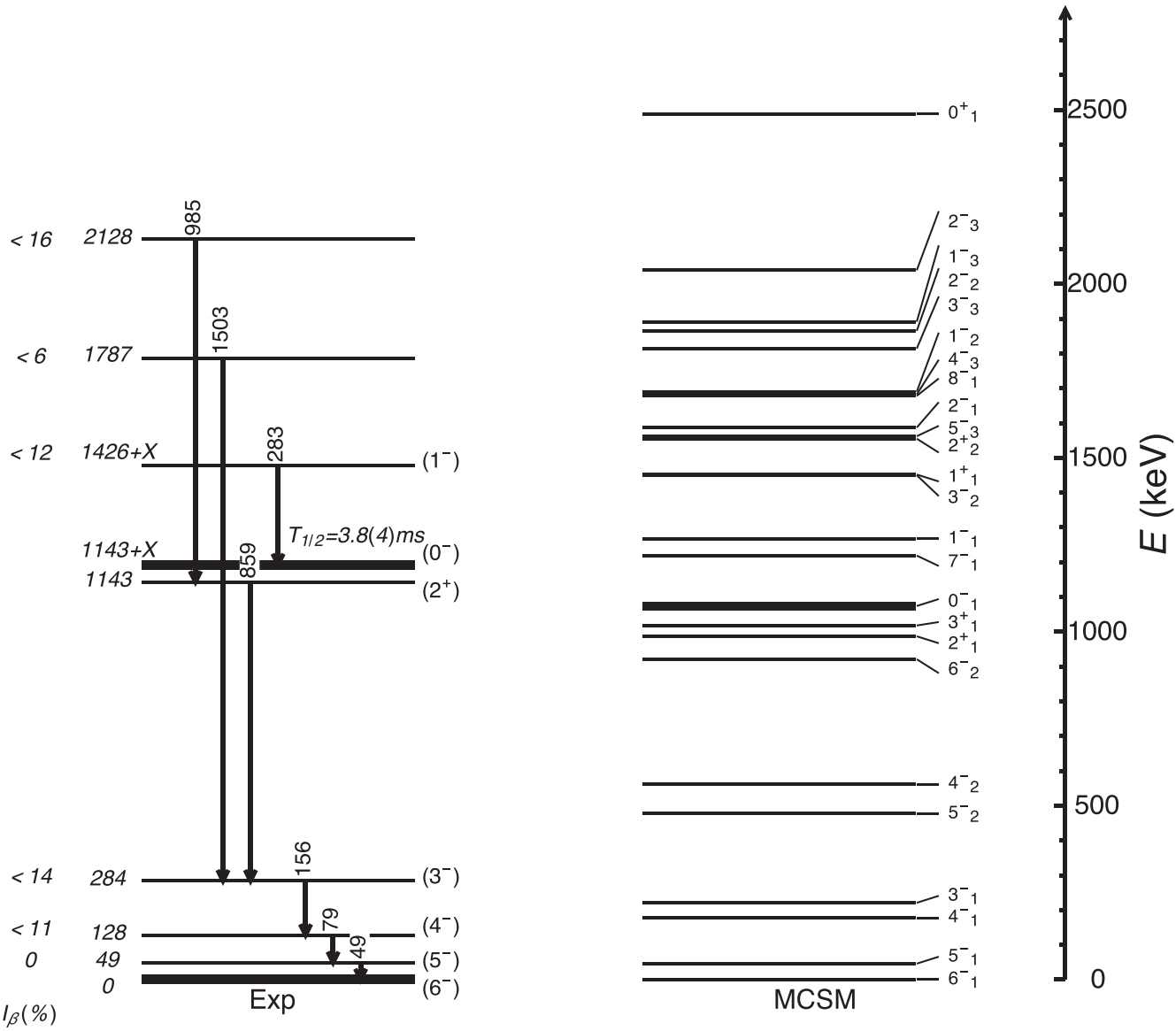

FIG. 3. Experimental level scheme for ^{78}Cu and comparison to MCSM calculations (see text for details).

of the three transitions are approximately the same when taking electron conversion into account and assuming $M1$ multipolarity. Other multipolarities for transitions between negative-parity states would result in significantly higher conversion coefficients. As an example, the conversion coefficient for a 49 keV transition of $M1$ multipolarity is 0.385, whereas it is 8.98 for $E2$ multipolarity [27]. Other multipolarities than $M1$ would therefore either require strong β feeding, which would be highly forbidden, or strong γ feeding that is only in coincidence with one or two transitions within the cascade, for which there is no evidence in the data. Higher multipolarity for transitions with such low energy would in addition result in relatively long lifetimes and delayed coincidences, whereas all three transitions are in prompt coincidence. It can therefore be concluded that the three strongest transitions form a cascade of $M1$ transitions feeding a (6^-) ground state from a (3^-) state at 284 keV. However, the data do not provide any indication for the ordering of the three transitions. According to the empiric rule established by Paar [14], the energies in proton-neutron multiplets with particle-hole character are expected to follow a parabolic trend with $I(I+1)$ and a minimum at spin $I = j_\pi + j_\nu - 1$, which is equal to six in the case of the $\pi 1f_{5/2} \times \nu 1g_{9/2}^{-1}$ configuration. With the ordering of the three transitions within the cascade as shown in the level scheme of Fig. 3, the states fit the expected parabolic trend well, which seems to justify this choice.

The singles spectrum in Fig. 1 shows a transition of 283 keV, and one would be tempted to place this transition as the decay from the 284 keV state. However, the 283 keV transition is not in coincidence with any of the transitions feeding the 284 keV state, as can be seen in Figs. 2(d) and 2(e). Furthermore, the transition would have $M3$ multipolarity if it was depopulating the 3^- state and would therefore unlikely be prompt. Any other ordering of spins for the low-energy states that would allow a prompt 283 keV transition would be in conflict with the observed intensities for the low-energy

TABLE I. γ-ray energies and intensities, along with their initial-state excitation energies, spin and parity, and β feeding.

E_γ (keV)	I_γ (%)	E_i	I^π	β feeding (%)
X		$1143 + X$	$(0v^-)$	
49(1)	43(4)[a]	49(1)	(5^-)	0
79(1)	44(1)[a]	128(2)	(4^-)	<11
156.1(2)	33(1)[a]	284(2)	(3^-)	<14
282.6(7)	12(1)	$1425.7 + X$	(1^-)	<12
464.5(5)	12(1)			
505(2)	9(1)			
575(3)	10(1)			
779.9(6)	7(1)			
859.0(6)	13(1)	1143(2)	(2^+)	
984.5(6)	16(1)	2128(2)		<16
1293(3)	2(2)			
1503(4)	6(2)	1787(4)		<6
1778(4)	3(2)			
1960(2)	2(1)			
2130(3)	2(1)			
2525(3)	2(1)			

[a]Corrected for internal conversion assuming pure $M1$ character.

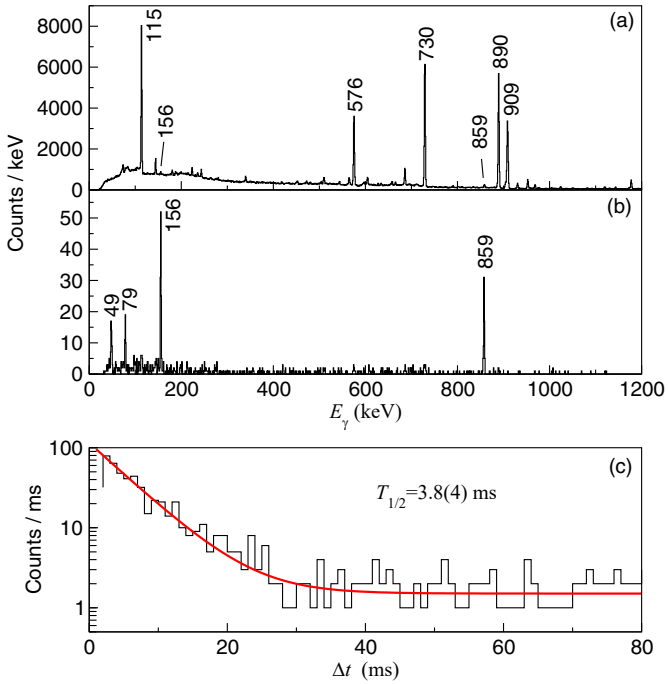

FIG. 4. (a) Decay spectrum of ^{78}Cu ions within 200 ms from implantation in the DSSSDs, revealing known transitions in ^{78}Zn and the 115 keV transition in ^{77}Zn. The small peaks at 156 and 859 keV, originating from excited states in ^{78}Cu, indicate the presence of an isomeric state. (b) Decay spectrum of ^{78}Cu within 5 ms, with an additional condition that a low-energy signal was detected in the same DSSSD pixel as the ion implantation. (c) Time difference between implantation of ^{78}Cu ions and detection of low-energy signals in the DSSSD, with an additional condition that one of the four γ-ray transitions following the decay of the isomer [as seen in spectrum (b)] was detected in EURICA. The exponential fit yields a half-life of $T_{1/2} = 3.8(4)$ ms.

transitions. It is therefore concluded that the 283 keV transition is originating from a state at higher excitation energy.

The 859, 985, and 1503 keV transitions were clearly seen in the γ-ray singles spectrum (see Fig. 1). Based on their time correlations with β decay, they can be identified as belonging to ^{78}Cu. All three transitions are in coincidence with the cascade of three low-energy transitions, as can be seen in Fig. 2. In addition, the 859 and 985 keV transitions are in mutual coincidence. Consequently, the 859 and 1503 keV transitions are placed on top of the (3^-) state at 284 keV excitation energy, and the 985 keV transition on top of the 859 keV transition, feeding a state at 1143 keV excitation energy. With only few transitions placed in the level scheme, the observed β feeding is incomplete and cannot be used for spin assignments. Because the higher-lying states are less likely to be affected by unobserved γ feeding, they are likely to have low spin. The proposed decay scheme is therefore consistent with bridging the large spin gap between states that are fed by allowed β transitions and a (6^-) ground state.

The analysis of time correlations in the decay of ^{78}Cu revealed clear evidence for an isomeric state, as is illustrated in Fig. 4. The spectrum in Fig. 4(a) shows γ rays following the implantation of ions identified as ^{78}Cu [$T_{1/2} = 330.7(20)$ ms] within 200 ms. As expected, the spectrum shows the known transitions in ^{78}Zn and ^{77}Zn [26]. The spectrum also shows hints of the 156 and 859 keV transitions originating from excited states in ^{78}Cu. When selecting a short correlation time of 5 ms, as shown in Fig. 4(b), the cascade of low-energy transitions and the 859 keV transition of ^{78}Cu appears in the spectrum. The spectrum of Fig. 4(b) was further cleaned by selecting events where a low-energy signal was detected in the same DSSSD pixel as the ion implantation, reducing the efficiency for β-decay events and enhancing events originating from conversion electrons. The delayed γ-ray spectrum shows the 859 keV transition, but not the one at 985 keV. This confirms the ordering of the cascade, and clearly shows that the isomeric state is located above the state at 1143 keV. The absence of the 283 keV transition in the delayed spectrum furthermore confirms that it does not originate from the (3^-) state. Because the 283 keV transition is relatively strong, but not seen in coincidence with any other transition, it seems likely that it is feeding the isomeric state.

The time spectrum of the isomeric decay is shown in Fig. 4(c), from which a half-life of $T_{1/2} = 3.8(4)$ ms can be extracted. The spectrum shows the time difference between the implantation of a ^{78}Cu ion and the detection of a low-energy signal in the same pixel of the DSSSD, with an additional condition that one of the four γ-ray transitions following the decay of the isomer was detected. The fact that the decay from the isomer to the state at 1143 keV remained unobserved could be explained by a small energy difference and consequently a large conversion coefficient, consistent with the conversion-electron signal observed in the DSSSD.

Any spin assignment with $I \geqslant 1$ for the isomer would be incompatible with the observed half-life of 3.8(4) ms. For a 1^+ state, for example, a $M2$ transition of at least 859 keV to the (3^-) state would likely result in a half-life of nanoseconds rather than milliseconds. A 1^- assignment or any higher spin would result in prompt decay to one of the low-lying states.

TABLE II. Occupation of proton and neutron orbitals in $fpg_{9/2}d_{5/2}$ spaces.

E (MeV)	J^π	$\pi 1f_{7/2}$	$\pi 2p_{3/2}$	$\pi 1f_{5/2}$	$\pi 2p_{1/2}$	$\pi 1g_{9/2}$	$\pi 1d_{5/2}$	$\nu 1f_{7/2}$	$\nu 2p_{3/2}$	$\nu 1f_{5/2}$	$\nu 2p_{1/2}$	$\nu 1g_{9/2}$	$\nu 1d_{5/2}$
0.000	6^-	7.73	0.25	0.96	0.02	0.04	0.01	7.99	3.99	5.99	1.99	8.86	0.19
0.046	5^-	7.71	0.33	0.87	0.03	0.04	0.01	7.99	3.99	5.99	1.99	8.85	0.20
0.178	4^-	7.71	0.35	0.84	0.05	0.04	0.01	7.99	3.99	5.99	1.98	8.83	0.21
0.221	3^-	7.74	0.46	0.73	0.02	0.04	0.01	7.99	3.99	5.99	1.99	8.86	0.18
0.477	5^-	7.70	0.87	0.30	0.07	0.04	0.01	7.99	3.99	5.99	1.98	8.84	0.21
0.562	4^-	7.74	0.84	0.34	0.03	0.04	0.01	7.99	3.99	5.99	1.98	8.85	0.19
0.921	6^-	7.71	0.95	0.25	0.03	0.05	0.01	7.99	3.98	5.99	1.98	8.88	0.18
0.987	2^+	7.63	0.26	1.04	0.02	0.04	0.01	7.99	3.92	5.92	1.15	9.78	0.24
1.018	3^+	7.60	0.26	1.07	0.02	0.04	0.01	7.99	3.95	5.88	1.15	9.76	0.26
1.074	0^-	7.58	0.29	1.03	0.05	0.04	0.01	7.98	3.92	5.92	1.89	8.13	1.15

Also a 0^+ assignment seems highly unlikely for the isomeric state. An $E3$ transition of at least 859 keV and a strength of 1 Weisskopf unit would result in a half-life of less than 10 μs, 500 times shorter than the observed value. The most likely assignment for the isomeric state is therefore 0^-. A possible $M3$ decay to the state at 284 keV would be sufficiently hindered for it to be unobserved. Instead, a low-energy decay to the state at 1143 keV would become competitive, consistent with the conversion electron signal in the DSSSD. The state at 1143 keV would in this case most likely have spin-parity $I^\pi = 2^+$. The half-life of 3.8(4) ms can be explained by an energy difference of ≈50 keV between the two states and a $M2$ transition of 1 Weisskopf unit. Such a transition would have a conversion coefficient of ≈6, consistent with the DSSSD signal and the nonobservation of a γ ray. Although it is not possible to determine the precise excitation energy of the isomeric state in this way, a 0^- assignment and a low-energy $M2$ transition of a few tens of keV to a 2^+ state at 1143 keV is the only scenario that can explain all observations.

The data are insufficient to determine whether the isomeric state is directly fed by β decay. It is likely that some of the prompt γ-ray transitions that were observed in the singles spectrum for ^{78}Cu feed the isomer. The fact that prompt coincidence relationships are lacking for the relatively strong 283 keV transition suggests that this transition is feeding the isomeric state directly. The resulting state has an excitation energy of $(1427 + X)$ keV, with X being the energy difference between the isomer and the state at 1143 keV.

V. DISCUSSION

To understand the nature of the experimentally observed states, shell-model calculations are necessary. In the present work, we compare the experimental results with Monte Carlo shell-model (MCSM) calculations [15] using the A3DA-m effective interaction, which has successfully described the structure of nuclei in the ^{78}Ni region [9,11,16,28]. The valence space comprised the full pf shell together with the $1g_{9/2}$ and $2d_{5/2}$ orbitals for both protons and neutrons without restrictions. Calculated states up to an excitation energy of 2.5 MeV, for both negative and positive parity, are compared with the experimental level scheme in Fig. 3. Table II shows the occupation numbers for protons and neutrons found in the MCSM calculations for the ten lowest states.

The calculations reproduce the sequence of negative-parity states that was established by the cascade of $M1$ transitions very well, including $I^\pi = 6^-$ for the ground state. The occupation numbers illustrate that these states have a relatively pure particle-hole character based on the $\pi 1f_{5/2} \times \nu 1g_{9/2}^{-1}$ configuration. This is consistent with the inversion of the $\pi 1f_{5/2}$ and $\pi 2p_{3/2}$ orbitals near $N = 48$, which was observed previously [9]. The calculations predict the remaining 2_1^- and 7_1^- members of the multiplet to be at much higher excitation energy, with the negative-parity states based on the $\pi 2p_{3/2} \times \nu 1g_{9/2}^{-1}$ configuration in between. The latter comprises the 5_2^-, 4_2^-, 6_2^-, and 3_2^- states.

The MCSM calculations predict a 0^- state at 1074 keV, close to the excitation energy of the observed isomeric state, which lends further support to the (0^-) assignment for the isomer. The calculations find a relatively pure $\pi 1f_{5/2}\nu 2d_{5/2}$ configuration for the 0^- state. The excitation energy of the isomeric state contains therefore not only information on the interaction energy between the $\pi 1f_{5/2}$ and $\nu 2d_{5/2}$ orbitals, but also on the size of the $N = 50$ shell gap. The good agreement between the experimental and theoretical excitation energy indicates that both quantities are well described by the A3DA-m interaction. The $\pi 1f_{5/2}\nu 2d_{5/2}$ configuration gives rise to a multiplet of negative-parity states comprising the 0_1^-, 1_1^-, 5_3^-, 4_3^-, 3_3^-, and 2_2^- states. The experimental state at $1427 + X$ keV excitation energy is a potential candidate for the 1_1^- state, as strong $M1$ transitions are expected between the states of the multiplet, although such an assignment remains speculative.

All calculated low-lying positive-parity states are based on a neutron excitation from the $\nu 2p_{1/2}$ to the $\nu 1g_{9/2}$ orbital. The coupling between an odd neutron in the $\nu 2p_{1/2}$ orbital and an odd proton in the $\pi 1f_{5/2}$ orbital results in a doublet of the 2^+ and 3^+ states. The occupation numbers of Table II show that the 2_1^+ and 3_1^+ states are indeed dominated by the $\pi 1f_{5/2}\nu 2p_{1/2}$ configuration. The experimental state at 1143 keV, which is tentatively assigned as (2^+), agrees reasonably well with the calculated 2_1^+ state at 987 keV and is consequently a candidate for a member of the $\pi 1f_{5/2}\nu 2p_{1/2}$ doublet. The coupling of a $\nu 2p_{1/2}$ neutron with a $\pi 2p_{3/2}$ proton results in a doublet of the 1_1^+ and 2_2^+ states, which are calculated to be at higher energy around 1.5 MeV. The calculated 0_1^+ state at approximately 2.5 MeV, finally, is found to be based on the $\pi 2p_{1/2}\nu 2p_{1/2}$ configuration. It would be

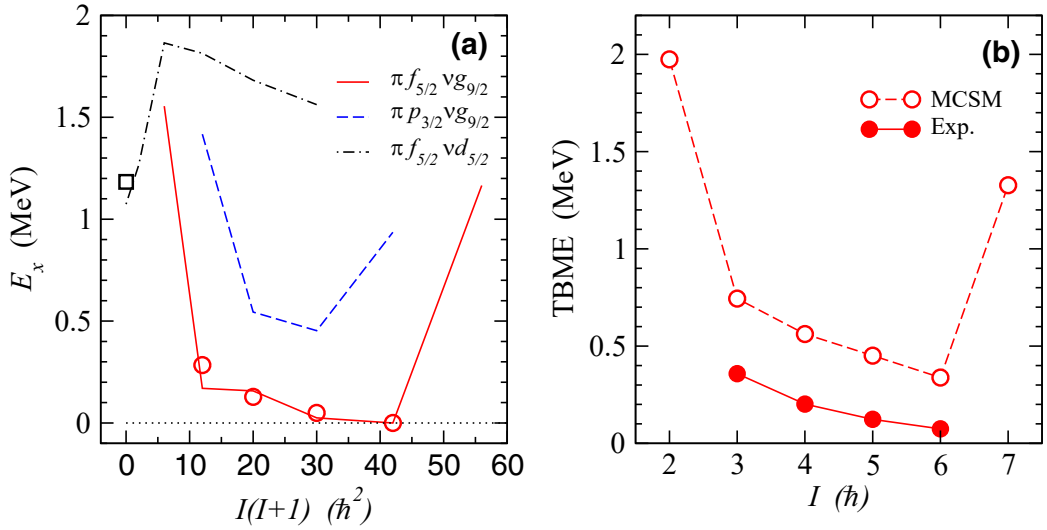

FIG. 5. (a) Excitation energies of the negative-parity multiplets with predominant $\pi 1f_{5/2}\nu 1g_{9/2}^{-1}$, $\pi 2p_{3/2}\nu 1g_{9/2}^{-1}$, and $\pi 1f_{5/2}\nu 2d_{5/2}$ configurations from the MCSM calculations as a function of $I(I+1)$. The symbols indicate the experimental excitation energies for those states for which a tentative spin assignment and association with the multiplet was possible. (b) Two-body matrix elements (TBME) extracted for the $\pi f_{5/2}\nu g_{9/2}^{-1}$ spin multiplet from both the experimental and calculated excited states (see text for details).

speculative to associate any of the higher-lying experimental states with any of the calculated states.

Figure 5(a) shows the excitation energies of the negative-parity states from the MCSM calculations as a function of the squared angular momentum $I(I+1)$. The calculated occupation numbers were used to assign the states to the multiplets with predominant $\pi 1f_{5/2}\nu 1g_{9/2}^{-1}$, $\pi 2p_{3/2}\nu 1g_{9/2}^{-1}$, and $\pi 1f_{5/2}\nu 2d_{5/2}$ configuration. Experimental excitation energies of states with a tentative spin assignment are also included in Fig. 5(a), which illustrates again the rather good agreement between the MCSM calculations and experiment. The multiplets involving a hole in the $\nu 1g_{9/2}$ orbital show a parabolic dependence on angular momentum, with the extreme couplings $I = j_\nu \pm j_\pi$ having the highest energy, as expected for particle-hole coupling [14]. The $\pi 1f_{5/2}\nu 2d_{5/2}$ multiplet, on the other hand, has particle-particle character, which favors (anti-)parallel coupling.

The observed excited states in the odd-odd Cu nuclei allow determining the proton-neutron monopole interaction, which is responsible for changes in single-particle energies, i.e., for the shell evolution far from stability. A description of the procedure to extract two-body matrix elements (TBMEs) from experimental excitation energies of proton-neutron multiplets can be found in Ref. [1]. In the following we apply this procedure for the case of ^{78}Cu. As can be seen in Table II, the negative-parity states of the $\pi 1f_{5/2}\nu 1g_{9/2}^{-1}$ multiplet have relatively pure single-particle (hole) configurations. The results are therefore well suited to extract experimental TBME for the interaction between a $1f_{5/2}$ proton with a $1g_{9/2}^{-1}$ neutron hole. Starting from a ^{78}Ni core, the contributions of a noninteracting proton particle and neutron hole are obtained from the binding energies of ^{79}Cu [5] and ^{77}Ni [23] for the $1f_{5/2}$ proton and the $1g_{9/2}$ neutron hole, respectively. The resulting value is found to be 74 keV lower than the experimental binding energy for the ground state of ^{78}Cu [29], which includes the repulsive residual interaction between the $1f_{5/2}$ proton and the $1g_{9/2}$ neutron hole when coupled to spin 6^-. The TBME for the various spin couplings are consequently shifted by 74 keV compared with the excitation energies of the corresponding states. It should be noted that the masses of ^{77}Ni and ^{78}Ni are not known experimentally, and that the extrapolated values have an uncertainty of 400 keV [23]. The absolute values of the experimental TBME depend therefore strongly on the extrapolated masses of the Ni isotopes. The experimental values are compared with TBME of the A3DA-m interaction in Fig. 5(b), where the theoretical TBME for the $\pi f_{5/2}\nu g_{9/2}^{-1}$ particle-hole interaction were obtained by applying the Pandya transformation [30] to the corresponding particle-particle TBME. The comparison shows that the A3DA-m interaction describes the relative size of the TBME well. The experimental results on the excited states in ^{78}Cu can be used to refine the shell-model interaction once more precise mass values for ^{77}Ni and ^{78}Ni become available.

VI. SUMMARY AND CONCLUSIONS

Excited states in ^{78}Cu have been observed for the first time following the β decay of ^{78}Ni. The neutron-rich ^{78}Ni isotopes were produced at the Radioactive Isotope Beam Factory at RIKEN Nishina Center, Japan, by in-flight fission induced by a primary beam of ^{238}U at 345 MeV per nucleon incident on a ^{9}Be target. The secondary beams were separated by the BigRIPS separator and transported to the decay station, where they were implanted into the WAS3ABi detector. The HPGe detectors of the EURICA array were used to detect γ rays following the β decay of ^{78}Ni. An isomeric state with a half-life of 3.8(4) ms was discovered in ^{78}Cu and tentatively assigned as (0^-). The combination of information from $\gamma\gamma$-coincidence data and the decay of the isomeric state allowed

building a partial level scheme for ^{78}Cu. Spins and parities could be tentatively assigned for some of the states.

The experimental results were compared with large-scale MCSM calculations using the A3DA-m interaction and a valence space comprising the $1f_{7/2}$, $2p_{3/2}$, $1f_{5/2}$, $2p_{1/2}$, $1g_{9/2}$, and $2d_{5/2}$ orbitals for both protons and neutrons. The shell-model calculations show a remarkable agreement with the experimental results. Combining the experimental results with the calculations, it was possible to interpret the low-lying states in terms of spin multiplets arising from the coupling of an odd proton in either the $\pi 1f_{5/2}$ or $\pi 2p_{3/2}$ orbital with an odd neutron in the $\nu 1g_{9/2}$, $\nu 2p_{1/2}$, or $\nu 2d_{5/2}$ orbital. The results confirm the previously observed crossing between the $\pi 2p_{3/2}$ and $\pi 1f_{5/2}$ orbitals. The interpretation of the isomeric state as based on the $\pi 1f_{5/2}$-$\nu 2d_{5/2}$ configuration provides information on the $N = 50$ shell gap. Because configurations are pure, it was possible to extract experimental two-body matrix elements for the $\pi 1f_{5/2}$-$\nu 1g_{9/2}^{-1}$ interaction, which represent important input for future shell-model calculations in the ^{78}Ni region. Extending the work to ^{80}Cu would represent an important step for investigating the proton-neutron interaction beyond ^{78}Ni.

ACKNOWLEDGMENTS

This work was carried out at the RIBF operated by RIKEN Nishina Center, RIKEN and CNS, University of Tokyo. This work was partially supported by KAKENHI (Grants No. 25247045, No. 23.01752, and No. 25800130). The authors acknowledge the EUROBALL Owners Committee for the loan of germanium detectors and the PreSpec Collaboration for the readout electronics of the cluster detectors. This work was partially supported by the Norwegian Research Council under project Contracts No. 240104, 262952, 263030, and 288061. The Monte Carlo shell-model calculations were performed on the K computer at RIKEN AICS (hp160211, hp170230, hp180179, hp190160). This work was supported in part by MEXT as "Priority Issue on Post-K Computer" (Elucidation of the Fundamental Laws and Evolution of the Universe) and as "Program for Promoting Researches on the Supercomputer Fugaku" (Simulation for basic science: from fundamental laws of particles to creation of nuclei) (hp200130) and JICFuS. Support from German BMBF Grant No. 05P19RDFN1 and No. 05P21RDFN1, from US DOE Grant No. DE-FG02-91ER-40609, from the National Research, Development and Innovation Fund of Hungary via Project No. K128947 and TKP2021-NKTA-42 is acknowledged. University of Brighton authors were supported by STFC Grant No. ST/J000132/1. This work was partially supported by Helmholtz Forschungsakademie Hessen für FAIR (HFHF), GSI Helmholtzzentrum für Schwerionenforschung, Campus Darmstadt, 64289 Darmstadt, Germany, and by Generalitat Valenciana, Conselleria de Innovación, Universidades, Ciencia y Sociedad Digital (CISEJI/2022/25).

[1] O. Sorlin and M.-G. Porquet, Prog. Part. Nucl. Phys. **61**, 602 (2008).
[2] T. Otsuka, A. Gade, O. Sorlin, T. Suzuki, and Y. Utsuno, Rev. Mod. Phys. **92**, 015002 (2020).
[3] R. Taniuchi, C. Santamaria, P. Doornenbal, A. Obertelli, K. Yoneda, G. Authelet, H. Baba, D. Calvet, F. Château, A. Corsi, A. Delbart, J.-M. Gheller, A. Gillibert, J. D. Holt, T. Isobe, V. Lapoux, M. Matsushita, J. Menéndez, S. Momiyama, T. Motobayashi *et al.*, Nature (London) **569**, 53 (2019).
[4] Z. Y. Xu, S. Nishimura, G. Lorusso, F. Browne, P. Doornenbal, G. Gey, H.-S. Jung, Z. Li, M. Niikura, P.-A. Söderström, T. Sumikama, J. Taprogge, Z. Vajta, H. Watanabe, J. Wu, A. Yagi, K. Yoshinaga, H. Baba, S. Franchoo, T. Isobe *et al.*, Phys. Rev. Lett. **113**, 032505 (2014).
[5] A. Welker, N. A. S. Althubiti, D. Atanasov, K. Blaum, T. E. Cocolios, F. Herfurth, S. Kreim, D. Lunney, V. Manea, M. Mougeot, D. Neidherr, F. Nowacki, A. Poves, M. Rosenbusch, L. Schweikhard, F. Wienholtz, R. N. Wolf, and K. Zuber, Phys. Rev. Lett. **119**, 192502 (2017).
[6] K.-L. Kratz, H. Gabelmann, P. Möller, B. Pfeiffer, H. L. Ravn, A. Wöhr, and The ISOLDE Collaboration, Z. Phys. A **340**, 419 (1991).
[7] S. Nikas, G. M. Pinedo, and A. Sieverding, J. Phys.: Conf. Ser. **1668**, 012029 (2020).
[8] K. T. Flanagan, P. Vingerhoets, M. Avgoulea, J. Billowes, M. L. Bissell, K. Blaum, B. Cheal, M. De Rydt, V. N. Fedosseev, D. H. Forest, C. Geppert, U. Köster, M. Kowalska, J. Krämer, K. L. Kratz, A. Krieger, E. Mané, B. A. Marsh, T. Materna, L. Mathieu *et al.*, Phys. Rev. Lett. **103**, 142501 (2009).
[9] E. Sahin, F. L. Bello Garrote, Y. Tsunoda, T. Otsuka, G. de Angelis, A. Görgen, M. Niikura, S. Nishimura, Z. Y. Xu, H. Baba, F. Browne, M.-C. Delattre, P. Doornenbal, S. Franchoo, G. Gey, K. Hadyńska-Klk, T. Isobe, P. R. John, H. S. Jung, I. Kojouharov *et al.*, Phys. Rev. Lett. **118**, 242502 (2017).
[10] C. Petrone, J. M. Daugas, G. S. Simpson, M. Stanoiu, C. Plaisir, T. Faul, C. Borcea, R. Borcea, L. Cáceres, S. Calinescu, R. Chevrier, L. Gaudefroy, G. Georgiev, G. Gey, O. Kamalou, F. Negoita, F. Rotaru, O. Sorlin, and J. C. Thomas, Phys. Rev. C **94**, 024319 (2016).
[11] L. Olivier, S. Franchoo, M. Niikura, Z. Vajta, D. Sohler, P. Doornenbal, A. Obertelli, Y. Tsunoda, T. Otsuka, G. Authelet, H. Baba, D. Calvet, F. Château, A. Corsi, A. Delbart, J.-M. Gheller, A. Gillibert, T. Isobe, V. Lapoux, M. Matsushita *et al.*, Phys. Rev. Lett. **119**, 192501 (2017).
[12] T. Otsuka, T. Suzuki, R. Fujimoto, H. Grawe, and Y. Akaishi, Phys. Rev. Lett. **95**, 232502 (2005).
[13] J. Van Roosbroeck, H. De Witte, M. Gorska, M. Huyse, K. Kruglov, D. Pauwels, J.-C. Thomas, K. Van de Vel, P. Van Duppen, S. Franchoo, J. Cederkall, V. N. Fedoseyev, H. Fynbo, U. Georg, O. Jonsson, U. Köster, L. Weissman, W. F. Mueller, V. I. Mishin, D. Fedorov *et al.*, Phys. Rev. C **71**, 054307 (2005).
[14] V. Paar, Nucl. Phys. A **331**, 16 (1979).
[15] N. Shimizu, T. Abe, Y. Tsunoda, Y. Utsuno, T. Yoshida, T. Mizusaki, M. Honma, and T. Otsuka, Prog. Theor. Exp. Phys. **2012**, 01A205 (2012).
[16] Y. Tsunoda, T. Otsuka, N. Shimizu, M. Honma, and Y. Utsuno, Phys. Rev. C **89**, 031301(R) (2014).

[17] K. Langanke, G. Martínez-Pinedo, J. M. Sampaio, D. J. Dean, W. R. Hix, O. E. B. Messer, A. Mezzacappa, M. Liebendörfer, H.-T. Janka, and M. Rampp, Phys. Rev. Lett. **90**, 241102 (2003).
[18] R. P. de Groote, J. Billowes, C. L. Binnersley, M. L. Bissell, T. E. Cocolios, T. Day Goodacre, G. J. Farooq-Smith, D. V. Fedorov, K. T. Flanagan, S. Franchoo, R. F. Garcia Ruiz, A. Koszorús, K. M. Lynch, G. Neyens, F. Nowacki, T. Otsuka, S. Rothe, H. H. Stroke, Y. Tsunoda, A. R. Vernon *et al.*, Phys. Rev. C **96**, 041302(R) (2017).
[19] P.-A. Söderström, S. Nishimura, P. Doornenbal, G. Lorusso, T. Sumikama, H. Watanabe, Z. Xu, H. Baba, F. Browne, S. Go, G. Gey, T. Isobe, H.-S. Jung, G. Kim, Y.-K. Kim, I. Kojouharov, N. Kurz, Y. Kwon, Z. Li, K. Moschner *et al.*, Nucl. Instrum. Methods Phys. Res., Sect. B **317**, 649 (2013).
[20] N. Fukuda, T. Kubo, T. Ohnishi, N. Inabe, H. Takeda, D. Kameda, and H. Suzuki, Nucl. Instrum. Methods Phys. Res., Sect. B **317**, 323 (2013).
[21] T. Kubo, D. Kameda, H. Suzuki, N. Fukuda, H. Takeda, Y. Yanagisawa, M. Ohtake, K. Kusaka, K. Yoshida, N. Inabe, T. Ohnishi, A. Yoshida, K. Tanaka, and Y. Mizoi, Prog. Theor. Exp. Phys. **2012**, 03C003 (2012).
[22] S. Nishimura, Prog. Theor. Exp. Phys. **2012**, 03C006 (2012).
[23] M. Wang, W. Huang, F. Kondev, G. Audi, and S. Naimi, Chin. Phys. C **45**, 030003 (2021).
[24] A. Tolosa Delgado, Ph.D. thesis, U. Valencia (main), 2020 (unpublished).
[25] C. J. Gross, J. A. Winger, S. V. Ilyushkin, K. P. Rykaczewski, S. N. Liddick, I. G. Darby, R. K. Grzywacz, C. R. Bingham, D. Shapira, C. Mazzocchi, S. Padgett, M. M. Rajabali, L. Cartegni, E. F. Zganjar, A. Piechaczek, J. C. Batchelder, J. H. Hamilton, C. T. Goodin, A. Korgul, and W. Królas, Acta Phys. Pol. B **40**, 447 (2009).
[26] A. Korgul, K. P. Rykaczewski, J. A. Winger, S. V. Ilyushkin, C. J. Gross, J. C. Batchelder, C. R. Bingham, I. N. Borzov, C. Goodin, R. Grzywacz, J. H. Hamilton, W. Królas, S. N. Liddick, C. Mazzocchi, C. Nelson, F. Nowacki, S. Padgett, A. Piechaczek, M. M. Rajabali, D. Shapira *et al.*, Phys. Rev. C **86**, 024307 (2012).
[27] T. Kibédi, T. Burrows, M. Trzhaskovskaya, P. Davidson, and C. Nestor, Nucl. Instrum. Methods Phys. Res., Sect. A **589**, 202 (2008).
[28] F. L. Bello Garrote, E. Sahin, Y. Tsunoda, T. Otsuka, A. Görgen, M. Niikura, S. Nishimura, G. de Angelis, G. Benzoni, A. I. Morales, V. Modamio, Z. Y. Xu, H. Baba, F. Browne, A. M. Bruce, S. Ceruti, F. C. L. Crespi, R. Daido, M.-C. Delattre, P. Doornenbal *et al.*, Phys. Rev. C **102**, 034314 (2020).
[29] S. Giraud, L. Canete, B. Bastin, A. Kankainen, A. Fantina, F. Gulminelli, P. Ascher, T. Eronen, V. Girard-Alcindor, A. Jokinen, A. Khanam, I. Moore, D. Nesterenko, F. de Oliveira Santos, H. Penttilä, C. Petrone, I. Pohjalainen, A. De Roubin, V. Rubchenya, M. Vilen *et al.*, Phys. Lett. B **833**, 137309 (2022).
[30] S. P. Pandya, Phys. Rev. **103**, 956 (1956).

Paper III

Experimental level scheme of ^{78}Cu

Acta Physica Polonica B Proceedings Supplement 16, 4-A14 (2023)

III

III

EXPERIMENTAL LEVEL SCHEME OF ^{78}Cu*

L.G. Pedersen[a], E. Sahin[a], A. Görgen[a], F.L. Bello Garrote[a]
Y. Tsunoda[b], T. Otsuka[c], M. Niikura[c], S. Nishimura[d], Z. Xu[c,e]
H. Baba[d], G. Benzoni[f], F. Browne[d,g], A.M. Bruce[g], S. Ceruti[f]
F.C.L. Crespi[f,h], R. Daido[i,d], G. de Angelis[j], M.-C. Delattre[k]
Zs. Dombradi[l], P. Doornenbal[d], Y. Fang[i,d], S. Franchoo[k], G. Gey[m]
A. Gottardo[j], T. Isobe[d], P.R. John[n], H.S. Jung[o], I. Kojouharov[p]
T. Kubo[d], N. Kurz[p], I. Kuti[l], Z. Li[q], G. Lorusso[d], I. Matea[k]
K. Matsui[c], D. Mengoni[n], T. Miyazaki[c], V. Modamio[a], S. Momiyama[c]
A.I. Morales[f,h,r], P. Morfouace[k], D.R. Napoli[j], F. Naqvi[s]
H. Nishibata[i], A. Odahara[i], R. Orlandi[t,u], Z. Patel[d,v], S. Rice[d,v]
H. Sakurai[c,d], H. Schaffner[p], L. Sinclair[d,w], P.-A. Söderström[d,x]
D. Sohler[l], I.G. Stefan[k], T. Sumikama[y], D. Suzuki[k], R. Taniuchi[b,w]
J. Taprogge[d,z], Z. Vajta[d,l], J.J. Valiente-Dobón[j], H. Watanabe[α]
V. Werner[s], J. Wu[d,q], A. Yagi[i,d], M. Yalcinkaya[β], R. Yokoyama[b]
K. Yoshinaga[γ]

[a]Department of Physics, University of Oslo, Norway
[b]Center for Nuclear Study, University of Tokyo, Japan
[c]Department of Physics, University of Tokyo, Japan
[d]RIKEN Nishina Center, Wako, Saitama, Japan
[e]University of Hong Kong, Hong Kong, China
[f]INFN, Sezione di Milano, Italy
[g]University of Brighton, United Kingdom
[h]Dipartimento di Fisica dell'Università degli Studi di Milano, Italy
[i]Department of Physics, Osaka University, Japan
[j]INFN, Laboratori Nazionali di Legnaro, Italy
[k]IPN, IN2P3-CNRS, Universite Paris-Sud, Orsay, France
[l]ATOMKI, Debrecen, Hungary
[m]LPSC, Universite Joseph Fourier, CNRS/IN2P3, Grenoble, France
[n]INFN Padova and Dipartimento di Fisica, Università di Padova, Italy
[o]Department of Physics, University of Notre Dame, USA
[p]GSI Darmstadt, Germany
[q]Department of Physics, Peking University, Beijing, China
[r]IFIC, CSIC-Universitat de València, Spain
[s]Yale University, New Haven, USA
[t]Instituut voor Kern- en StralingsFysica, K.U. Leuven, Belgium
[u]Advanced Science Research Center, JAEA, Tokai, Japan
[v]Department of Physics, University of Surrey, United Kingdom
[w]Department of Physics, University of York, United Kingdom
[x]ELI-NP and IFIN-HH, Bucharest, Romania
[y]Department of Physics, Tohoku University, Sendai, Japan
[z]CSIC, Madrid, Spain
[α]Beihang University, Beijing, China
[β]Department of Physics, Istanbul University, Turkey
[γ]Department of Physics, Tokyo University of Science, Chiba, Japan

Received 1 December 2022, accepted 6 February 2023, published online 22 March 2023

* Presented at the Zakopane Conference on Nuclear Physics, *Extremes of the Nuclear Landscape*, Zakopane, Poland, 28 August–4 September, 2022.

Excited states in ^{78}Cu were observed for the first time following the β decay of ^{78}Ni created by in-flight fission of ^{238}U. Based on the coincidence relationships between the observed γ-ray transitions, it was possible to construct a level scheme comprising eight excited states with tentative spin assignments for 5 of them. In addition to the γ-decaying states, an isomeric state with a lifetime of 3.8(4) ms was found to decay by internal conversion.

DOI:10.5506/APhysPolBSupp.16.4-A14

1. Introduction

The doubly magic ^{78}Ni represents an important benchmark for nuclear structure studies, providing information on the consequences of a large neutron excess. The properties of nuclei in the region of ^{78}Ni are furthermore important for the understanding of the astrophysical r-process. With one additional proton and one neutron hole relative to ^{78}Ni, ^{78}Cu is an ideal nucleus to study the proton–neutron interaction in this region of the nuclear chart. Probing the structure of ^{78}Cu can therefore reveal important aspects of nuclear structure beyond ^{78}Ni. Previous studies of odd–even $^{69-79}$Cu have shown that the proton $p_{3/2}$ and $f_{5/2}$ orbitals shift in energy and cross when moving away from stability and approaching $N = 50$ [1–3]. Low-energy states in ^{78}Cu are therefore expected to form a multiplet based on the coupling of the $\pi f_{5/2}$ and $\nu g_{9/2}^{-1}$ orbitals. Given the large spin differences that may arise from the multiplet structure in odd–odd nuclei, isomeric states are common and may also be expected in ^{78}Cu.

2. Experimental details and results

The experiment took place at the RIKEN Nishina Center, Saitama, Japan, during the EURICA campaign [4]. A beam of ^{238}U at 345 MeV/u was incident on a ^{9}Be target, producing a wide range of fission fragments, which were separated and identified in the BigRIPS fragment separator. The separator was optimized for the transmission of nuclei in the vicinity of ^{78}Ni, and ions of interest were implanted into the WAS3ABi array of DSSSD detectors, which was surrounded by the EURICA array of HPGe detectors.

In the first step of the analysis procedure, the β-decay half-life of ^{78}Ni was determined. Figure 1 shows the total decay curve for ^{78}Ni, corresponding to the time difference between ion implantation and detection of β-decay electrons within the same or neighboring pixel of WAS3ABi. The decay curve contains not only β-decay events from ^{78}Ni, but also subsequent daughter decays, including those populated by beta-delayed neutron emission. The known half-lives and probabilities for neutron emission P_n [5] for the daughter decays were fixed in the fitting procedure, leaving only the half-life of

^{78}Ni and the total number of decay events as free parameters. The latter can be used to determine the detector efficiency and is needed to determine decay intensities. The half-life of ^{78}Ni was found to be 122.2(51) ms [6]. Details of the procedure can be found in Ref. [7].

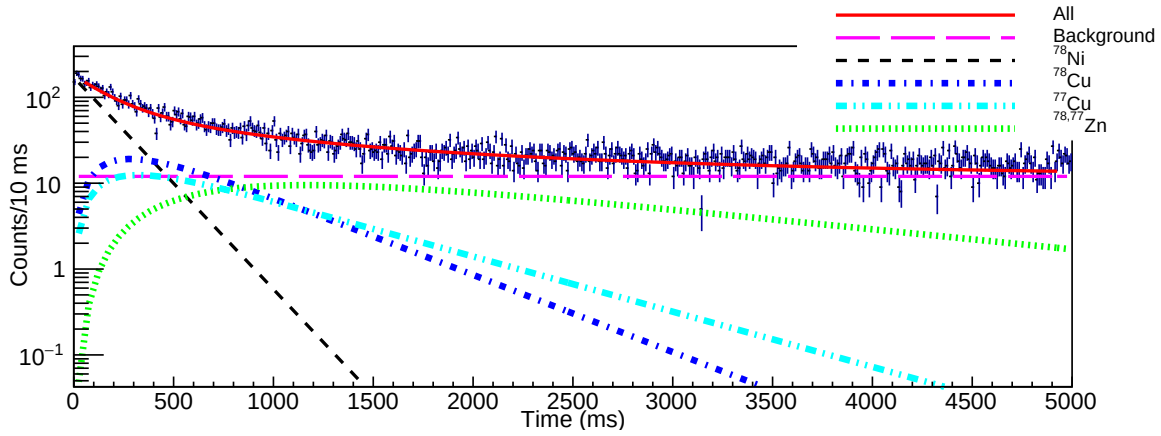

Fig. 1. Total observed number of detected beta decays fitted with the corresponding number of decays from implanted ^{78}Ni and its daughters and grand-daughters.

Based on the time correlations between ion implantation and β decay, it was possible to associate γ-ray transitions with the decay of excited states in ^{78} is show γ

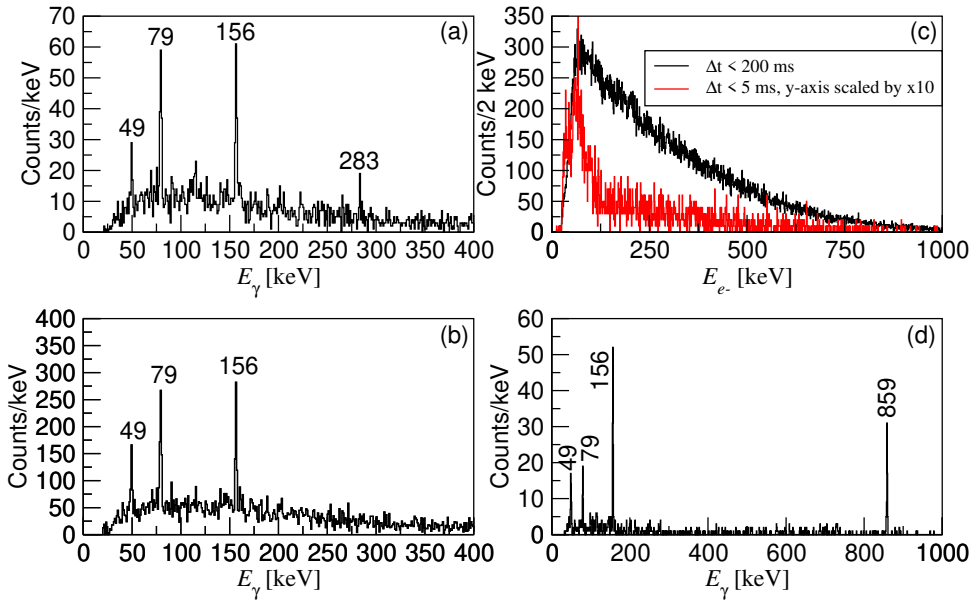

Fig. 2. (Color online) (a) Single γ-ray spectrum. Peaks are marked by their energy in keV. (b) Total projection γ–γ coincidence spectrum. (c) DSSSD signals for 200 ms (black) and 5 ms (red/gray, and scaled by a factor of 10 to clearly be seen in the figure). (d) γ-ray spectrum gated on low-energy DSSSD events below 200 keV and using a short time-gate of 5 ms.

coincidences and place several of the observed transitions in a level scheme for ^{78}Cu, which is shown in Fig. 3. The three low-energy transitions at 49, 79, and 156 keV are in prompt mutual coincidence with each other, and in coincidence with the 859, 985, and 1503 keV transitions. Being by far the strongest transitions, it is reasonable to assume that the cascade of low-energy transitions is feeding the ground state, which has been tentatively assigned as $I^\pi = (6^-)$ in a previous experiment [8]. The three low-energy transitions have comparable intensities when correcting for detector efficiency and electron conversion for M1 multipolarity. Other multipolarities for any of the low-energy transitions would result in long lifetimes of the states and much higher conversion coefficients, requiring a significant imbalance in either β or γ feeding, for which there is no evidence in the data. It is, therefore, concluded that the three low-energy transitions form a cascade of M1 transitions from a (3^-) state at 284 keV to the (6^-) ground state. Although there is no experimental indication for the ordering of the three transitions, the empiric parabolic rule for proton–neutron multiplets [9] suggests an ordering as shown in Fig. 3. These negative-parity states are interpreted as members of the $\pi f_{5/2} \times \nu g_{9/2}^{-1}$ multiplet. The remaining 2^- and 7^- members of the multiplet are unobserved and expected to lie at higher excitation energy. The 859 and 985 keV transitions are in mutual coincidence and therefore placed as a cascade feeding the (3^-) state. Besides the three low-energy transitions, no coincident γ rays were observed for the 1503 keV transition, which is consequently also assumed to be feeding the (3^-) state. Due to the lack of further coincidence relations and the resulting incompleteness of the level scheme, it would be highly speculative to attempt spin assignments for the higher-lying states.

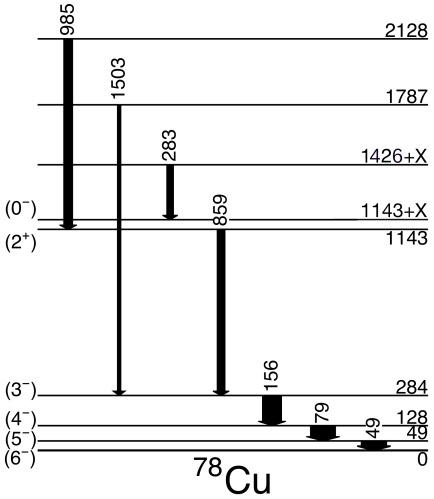

Fig. 3. Experimentally obtained level scheme.

The three low-energy transitions and the 859 keV transition are seen as weak lines in the decay following the implantation of ^{78}Cu, which suggests that they depopulate an isomeric state in ^{78}Cu. Figure 2 (c) shows the energy signals in WAS3ABi during the first 5 ms after implantation (red/gray) and during the first 200 ms after implantation (black). The low-energy signal in the spectrum for short correlation time is consistent with the detection of conversion electrons from a low-energy transition, whereas the spectrum for the longer correlation time is characteristic for β-decay electrons. Gating on the low-energy electron signal and short correlation times below 5 ms results in a very clean γ-ray spectrum showing the 49, 79, 156, and 859 keV transitions in ^{78}Cu, as shown in Fig. 2 (d). This is a clear proof of an isomeric state at a small energy above the state at 1143 keV excitation energy, and it determines the ordering of the 859 and 985 keV transitions. With a clean tag on γ rays and electron energy, the lifetime of the isomeric state was found to be 3.8(4) ms. Based on the lifetime of the isomeric state, together with the observation of conversion electrons and the non-observation of γ rays, the transition that depopulates the isomer is most likely of M2 multipolarity. The isomeric state is therefore interpreted as a (0^-) state based on the $\pi f_{5/2} \times \nu d_{5/2}^{-1}$ configuration, with the state at 1143 keV excitation energy assigned as (2^+). This interpretation is supported by shell model calculations [10].

The γ-ray singles spectrum shows a clear peak at 283 keV, as can be seen in Fig. 2 (a). One could be tempted to place the transition in parallel to the cascade of three low-energy transitions, as it corresponds approximately to the energy sum of the three transitions. However, the 283 keV transition has no coincidence relation with any other transition. This can be seen from its absence in the total projection of the γ–γ coincidence matrix, which is shown in Fig. 2 (b). Given the strength of the 283 and 859 keV transitions in the singles spectrum, any coincidence relation between them should have been observed. The absence of coincidences suggests that the 283 keV transition is feeding the isomeric state. More details and evidence will be presented in a forthcoming publication, together with a comparison to shell model calculations [10].

3. Conclusions

To summarize, ^{78}Cu has been studied by analyzing γ rays following the β decay of ^{78}Ni, produced by in-flight fission. A γ–γ coincidence analysis allowed constructing a partial level scheme for ^{78}Cu, comprising eight excited states. A sequence of low-lying states is interpreted as members of the $\pi f_{5/2} \times \nu g_{9/2}^{-1}$ multiplet. The energies of these states provide direct information on the proton–neutron interaction outside ^{78}Ni. In addition, an

isomeric state with a half-life of 3.8(4) ms has been observed to decay by electron conversion. This state is tentatively assigned as (0^-) and interpreted as based on the $\pi f_{5/2} \times \nu d_{5/2}^{-1}$ configuration, providing information on the size of the $N = 50$ shell gap.

This work was partially supported by KAKENHI (grants Nos. 25247045, 23.01752, and 25800130). The authors acknowledge the EUROBALL Owners Committee for the loan of germanium detectors and the PreSpec Collaboration for the readout electronics of the cluster detectors. This work was partially supported by the Norwegian Research Council under project contracts 240104, 262952, 263030, 288061, and 325714. Support from the German BMBF grants Nos. 05P19RDFN1 and 05P21RDFN1, from the U.S. DOE grant No. DE-FG02-91ER-40609, from the National Research, Development and Innovation Fund of Hungary via project No. K128947 and TKP2021-NKTA-42 is acknowledged. The University of Brighton authors were supported by STFC grant No. ST/J000132/1. This work was partially supported by the Helmholtz Forschungsakademie Hessen für FAIR (HFHF), GSI Helmholtzzentrum für Schwerionenforschung, Campus Darmstadt, 64289 Darmstadt, Germany, and Generalitat Valenciana, Conselleria de Innovación, Universidades, Ciencia y Sociedad Digital (CISEJI/2022/25).

REFERENCES

[1] K.T. Flanagan *et al.*, *Phys. Rev. Lett.* **103**, 142501 (2009).

[2] E. Sahin *et al.*, *Phys. Rev. Lett.* **118**, 242502 (2017).

[3] L. Olivier *et al.*, *Phys. Rev. Lett.* **119**, 192501 (2017).

[4] P.-A. Söderström *et al.*, *Nucl. Instrum. Methods Phys. Res. B* **317**, 649 (2013).

[5] A. Tolosa Delgado, «Study of beta-delayed neutron emitters in the region of ^{78}Ni and its impact on r-process nucleosynthesis», Ph.D. Thesis, Universitat de València (main), 2020.

[6] Z.Y. Xu *et al.*, *Phys. Rev. Lett.* **113**, 032505 (2014).

[7] Z.Y. Xu, «Beta-decay spectroscopy on neutron-rich nuclei in a range of $Z = 26$–32», Ph.D. Thesis, Department of Physics, University of Tokyo, 2014, http://hdl.handle.net/2261/57714

[8] R.P. de Groote *et al.*, *Phys. Rev. C* **96**, 041302 (2017).

[9] V. Paar *et al.*, *Nucl. Phys. A* **331**, 16 (1979).

[10] L.G. Pedersen *et al.*, accepted for publication in *Phys. Rev. C*.

Paper IV

Spectroscopy of ^{126}Sn following two-neutron transfer: Evidence for an excited 0^+ state

To be submitted to PRC

IV

Part III

Analysis details, summary and outlook

Chapter 3

Detailed analysis

In scientific articles there is not always room (or interest) to include every aspect of the data analysis. Sometimes, months of work is summarised in only a sentence or two. In this chapter more details on some of these aspects are presented. For the Cu analysis, this will mostly focus on how the β-decay half-lives and the number of ions were obtained, and describe the hunt for isomeric states. For the Sn analysis, this will focus on the data calibration process and the different gates used to clean the spectra.

3.1 Cu analysis

In order to properly determine the absolute intensities of γ-ray transitions, the total number of β-decaying ions of interest are needed. In the first two papers, these numbers are presented in tables but not discussed any further. First, the number of background decay events were fitted by studying events with negative time-stamps, i.e. decays that were detected before the implantation of an ion in the WAS3ABi detector, which can only be explained as random background. To obtain the number of β decays from the Ni isotopes of interest, the decay curve was fitted using the Bateman equations. The production and decay of each nuclide within a decay chain is described by a differential equation using the half-lives of the decays. The total number of β decays are known from the data. In the fit, the number of implanted Ni ions and their half-life were treated as free parameters. Ratios of β-delayed neutron emission are also included. The procedure is presented in Paper III, where the results of the ^{78}Cu case is shown. Similar fits are shown for ^{74}Cu in Figure 3.1 and ^{76}Cu in Figure 3.2. Table 3.1 also presents the number of β-decay events assigned to the different nuclei and the background events.

3.1.1 Identification of γ-lines

To identify peaks originating from the Cu isotopes under study, the time correlation between the ion implantation and the β and γ decay detection was exploited. When sorting data to obtain γ spectra, only γ rays following the first detected β-decay signal were included, whereas γ rays following any subsequently detected β-decay signal were excluded. If the efficiency of the β detector had been

Table 3.1: Results from the fitting procedures to obtain the half-life of ^{74}Ni and ^{76}Ni, and the number of detected β decays assigned to each isotope within the 5 s time window.

$A = 74$		$A = 76$	
$T_{1/2}$	502(2) ms	$T_{1/2}$	241(2) ms
Total	302.9×10^3	Total	540.4×10^3
Background	165.0×10^3	Background	156.0×10^3
^{74}Ni	75.5×10^3	^{76}Ni	267.2×10^3
^{74}Cu	56.7×10^3	^{76}Cu	96.3×10^3
^{73}Cu	3.8×10^3	^{75}Cu	12.2×10^3
^{74,73}Zn	1.4×10^3	^{76,75}Zn	2.8×10^3

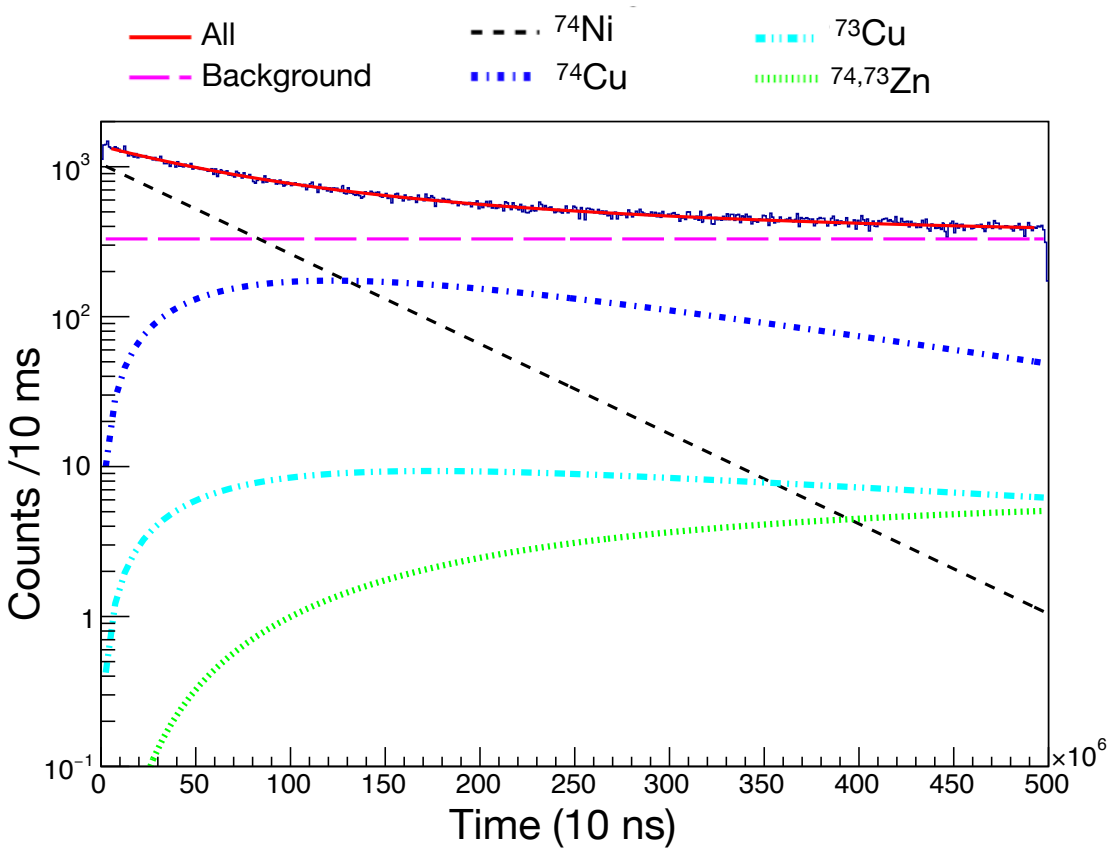

Figure 3.1: Fit of the decay curve for ^{74}Ni.

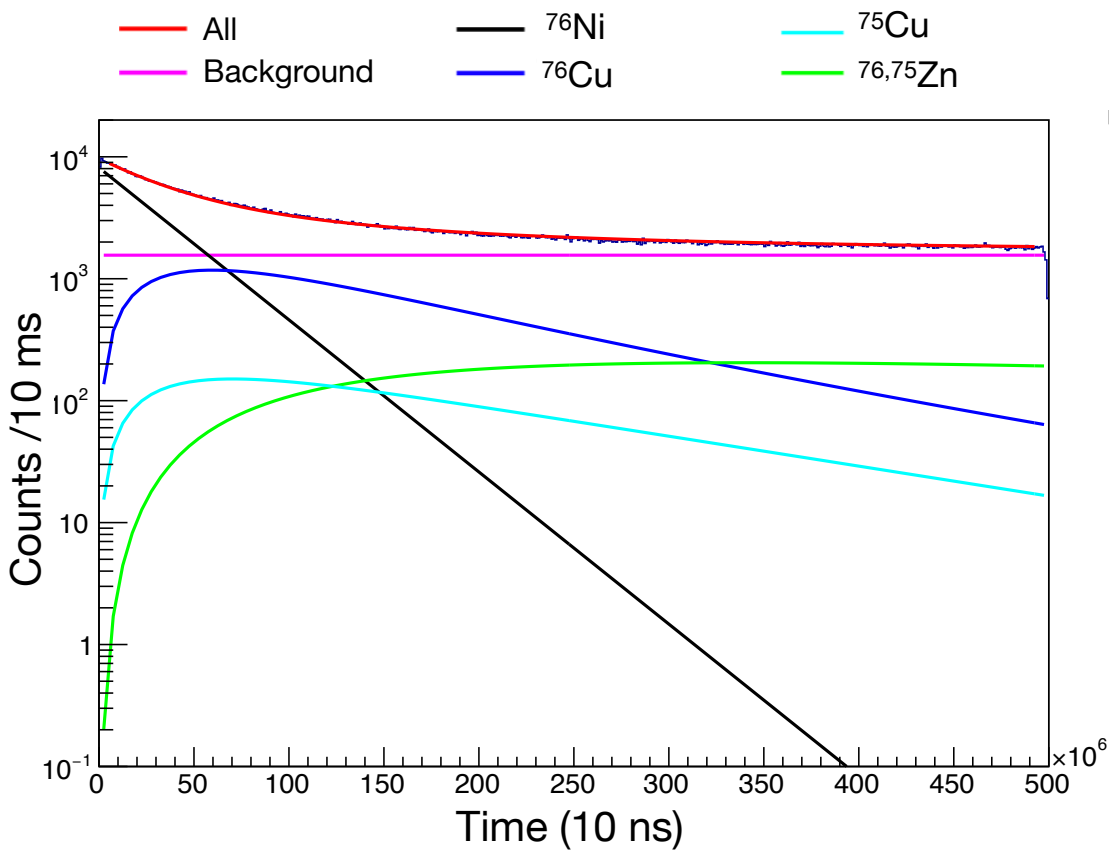

Figure 3.2: Fit of the decay curve for ^{76}Ni.

100% and it was possible to correctly associate all β-decay events with the nuclei that emitted them, this would in theory be enough to exclude all events from further β decays of the Cu isotopes. However, this is not the case, and even when only including the first β decays there can still be contamination from daughter decays, as the initial decay of the Ni mother might have been undetected. The restriction also does not differentiate between normal β decay and β-n emissions, and thus there can be contaminations from the $^{A-1}$Cu nucleus in the ^{A}Cu spectra. In order to separate peaks from contaminants and the Cu isotope under study, the time-window between the implantation of an ion and its subsequent β decay can be reduced the same scale as the half life of the isotope. For the various spectra studied during the analysis, we had to find a compromise between high statistics and clean spectra with good suppression of the daughter decays.

Figure 3.3 shows the difference between two ^{76}Cu spectra with different time-windows, while all other conditions were kept the same. The spectrum in a) is produced with a time-window of 200 ms, slightly below the half life of ^{76}Ni. The spectrum in b) is made with a time-window of 2 s, which is approximately ten times the half life. In the 200 ms spectrum, only ^{76}Cu peaks are clear peaks standing out from the background, in addition to the 599 keV peak from ^{76}Zn. In the 2 s spectrum the overall statistics is increased, but the ^{76}Zn peaks are much more prominent. Here, the ^{76}Zn 599 keV peak is the fourth biggest peak, and other ^{76}Zn peaks like the 698 peak are also clearly visible. By carefully studying the difference in relative strength as a function of the time window between ion implantation and β-decay detection, peaks could be either assigned to the Cu isotope under study, or to its daughter isotope. This is how some peaks could be assigned to the respective Cu isotopes without sufficient coincidence statistics to place them in the level schemes. The 340 keV peak, which is a transition in both ^{76}Cu and ^{76}Zn is a clear peak in the 200 ms spectrum, but also increases more than other ^{76}Cu peaks in the 2 s spectrum. The relative increase of this peak had to be studied in order to obtain the intensity of this peak stemming only from the decay in ^{76}Cu. This was done by measuring the peak area and studying the ratio of the 340 keV peak and the 480, and 1052 keV transitions in the 200 ms spectrum. Assuming that the ratio between the transitions remains constant, the areas of the same peaks could then be measured in the γ-ray spectrum with the wider time gate. The intensity of the 340 keV transition stemming only from ^{76}Cu is then obtained by using the ratios found in the 200 ms spectrum. Another peak that does not follow the characteristic time dependence of the ^{76}Ni or the ^{76}Cu β decay is the 75 keV peak. This is a known X-ray from Pb, arising from interactions with Pb shielding in the experimental hall. Due to the lack of coincidences and its characteristic energy seen in all spectra with the same relative intensity, it is safe to conclude that this indeed is an X-ray contamination peak.

3.1.2 Searching for isomeric states

Previous studies have found indications for an isomeric excited state in ^{76}Cu at 64.1 keV [40, 41], as mentioned in Paper I. No previous studies have found any indications for isomeric states in ^{74}Cu and ^{78}Cu. Energy-time matrices can be

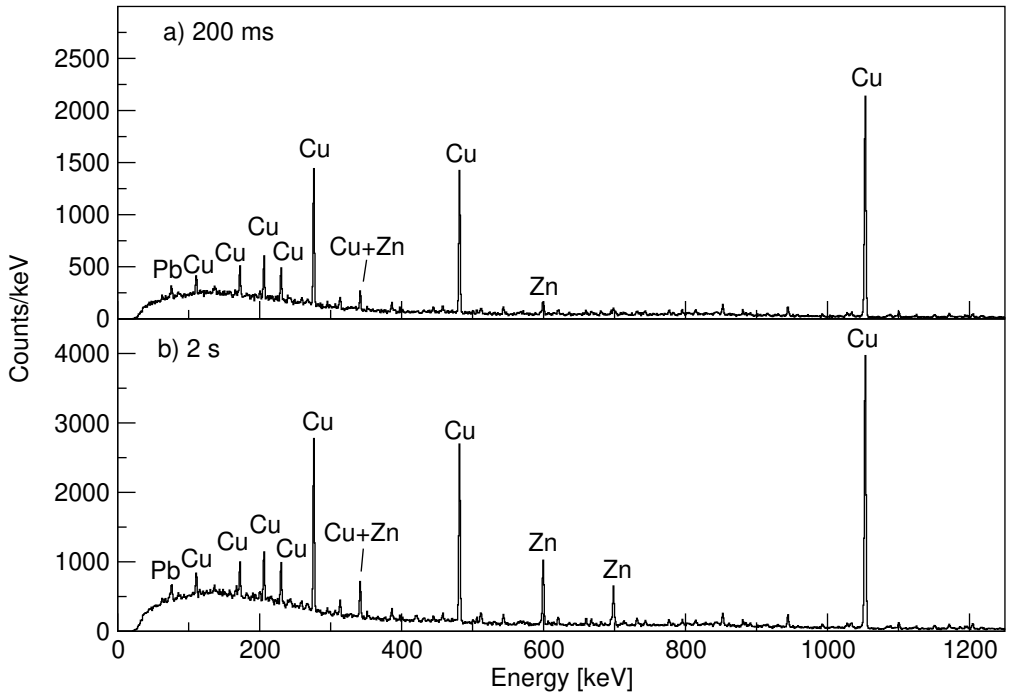

Figure 3.3: Example spectra for ^{76}Cu showing the difference between a 200 ms spectrum (a) and a 2 s spectrum (b). In the 2 s spectrum, known ^{76}Zn transitions like 599 keV and 698 keV are much bigger peaks compared to in the 200 ms spectrum. Peaks originating from ^{76}Cu have the same relative strengths in both spectra.

created to look for isomeric states. In these types of spectra, every γ-detection event is plotted based on the detected energy and time difference between the detection of a γ ray (start signal) and a common stop signal. Because of this sorting, time runs backwards in the plot, and any isomers would be seen as a longer tail towards smaller time values. Energy-time matrices are shown for all three nuclei in Figures 3.4-3.6. Note that the ^{78}Cu data is from a slightly different initial data sorting (by M. Niikura) than the ^{74,76}Cu (by Z. Xu), resulting in different time value scales. If any of the transitions were isomers, we would see a longer tail towards smaller time values. In ^{76}Cu, there seems to be a low-energy isomeric state, as the tail is stretched down towards zero. However, upon further inspection this stems from X-ray contaminations from Pb at 75 keV. In other words, the isomeric state at 64 keV is not seen in the current experiment. It is however hard to determine if this is because the isomer is not populated in β decay or if the statistics are simply too low. It can be noted that the MCSM calculations presented in Paper I include high spin states at low energy with $I = 4^-, 5^-, 6^-$. It is thus not unreasonable to think that such a low-energy state at 64.1 keV with a high spin will be only weakly (or not at all) populated in β-decay from a 0^+ ground state.

For ^{78}Cu, there is less data and no indications of isomers from the energy-time matrix in Figure 3.6, although this is a matrix with relatively low statistics overall. However, there is an isomeric state in ^{78}Cu that could only be seen through another method. This state is seen when analysing the data from β-decay of ^{78}Cu

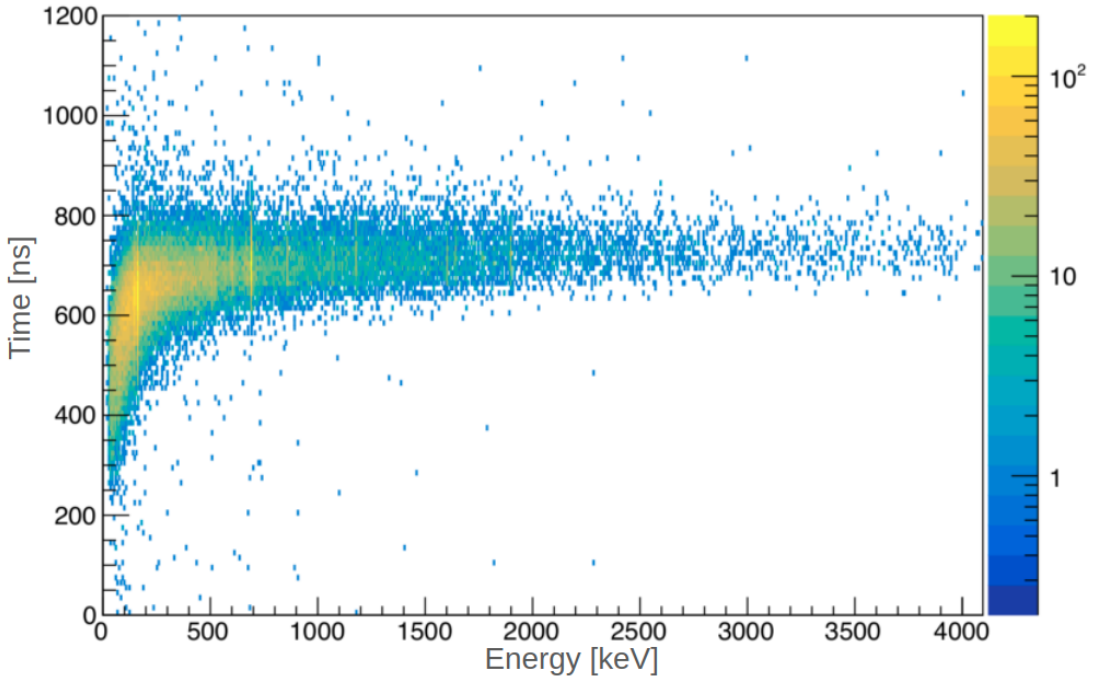

Figure 3.4: Energy-time matrix for ^{74}Cu.

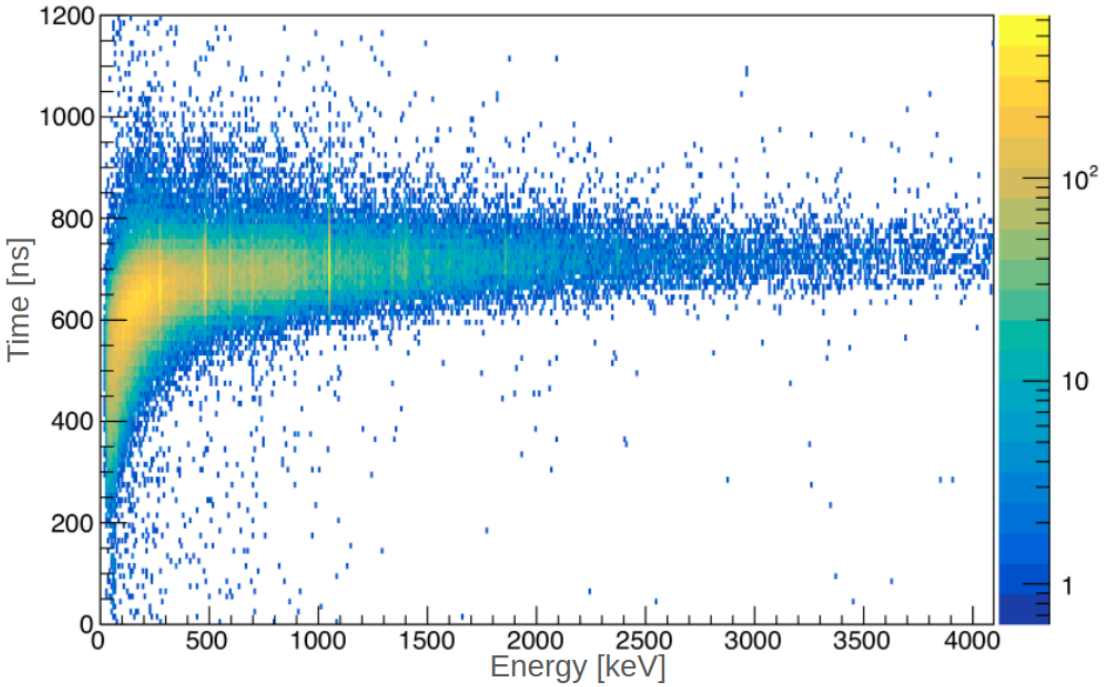

Figure 3.5: Energy-time matrix for ^{76}Cu.

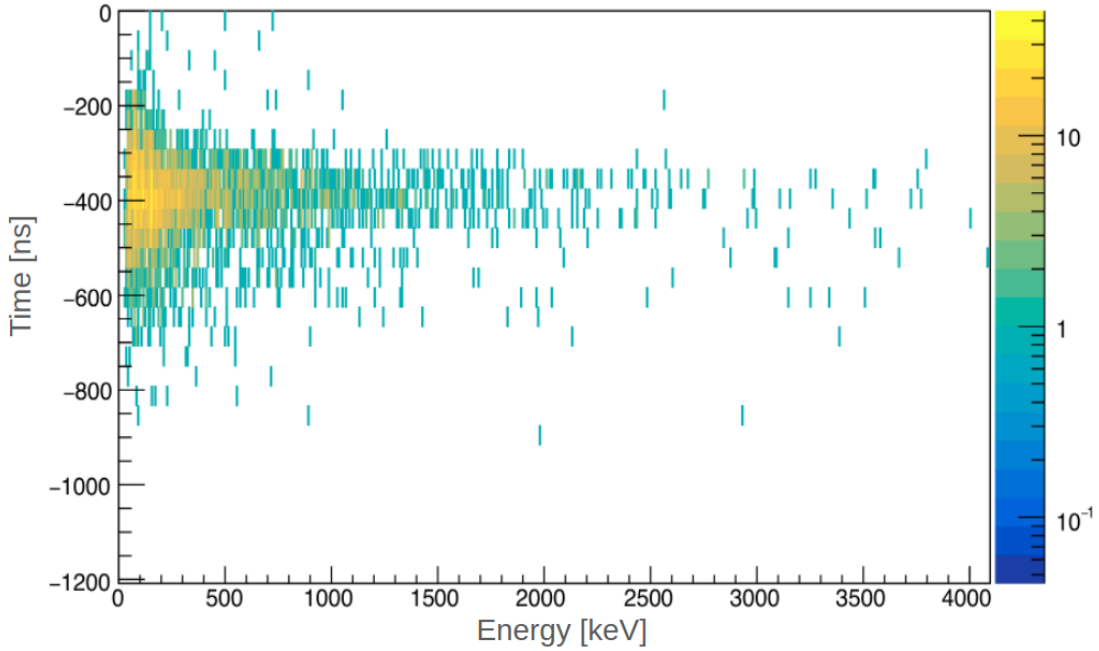

Figure 3.6: Energy-time matrix for ^{78}Cu.

implanted in the decay station, instead of the data of implanted ^{78}Ni. Evidence for the isomeric state was first observed by Zhengyu Xu, who is a co-author of the Cu paper and has been working on the data from the same experiment (among many others as well) to measure their lifetimes using the data from the EURICA campaign. While working on his own thesis, he saw indications of an isomeric state in ^{78}Cu when working on data of implanted ^{78}Cu, initially used to study ^{78}Zn, but did not follow up with a detailed analysis of the state. He reported his observation to us while we were working on the ^{78}Cu data. To further investigate the isomeric state and determine its properties, we received the data corresponding to the implementation of ^{78}Cu which was not a part of our original data sets, and could then properly study and characterise the isomer. Our results gave firm evidence for an isomeric state of 3.8(4) ms above 1143 keV, as presented and discussed in Paper II.

In Paper II, we also discuss the 283 keV peak that is seen in the single γ-ray spectrum, but not in the γ-γ coincidence matrix. 283 keV is close to the sum of the 156, 79, and 49 keV transitions, and could naively be interpreted as a parallel transition to this cascade. However, as the transition is not in coincidence with any other prompt transition, it is concluded that this transition feeds into the isomeric state at $X + 1143$ keV. The γ-ray singles spectrum is compared to the total projection of the γ-γ coincidence matrix in Figure 3.7.

After discovering the isomeric state, a crucial discussion was regarding its spin. The long lifetime of the isomeric state and the fact that it does not decay by γ rays to any of the low-lying states in ^{78}Cu suggested 0^- as the most likely spin-parity assignment, as discussed in Paper II. The original SM calculations did not consider 0^- states, but new calculations found a 0^- state at a similar energy that is consistent with the experimental results.

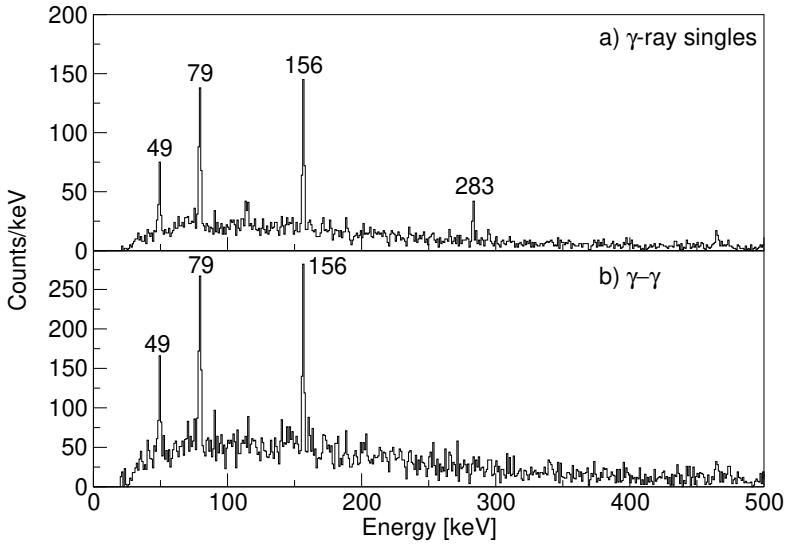

Figure 3.7: ^{78}Cu singles spectrum (a) and the total projection of the $\gamma\gamma$ matrix (b). Because the 283 keV peak is not seen in coincidence with any other transitions in ^{78}Cu, it is concluded that this transition feeds directly into the isomeric state. The singles spectrum is created with a stricter time gate to exclude contamination lines, while the γ-γ matrix is made with a wider time gate to not exclude events from ^{78}Cu.

3.2 Details on the analysis of ^{126}Sn

3.2.1 Calibration

Runs with ^{152}Eu and ^{56}Co were performed before inserting the ^{124}Sn target for γ-ray energy calibration. However, when doing the calibration later, it became evident that the peaks from ^{152}Eu were much smaller than the ^{56}Co ones. Instead of performing the energy calibration with ^{152}Eu and ^{56}Co, other known lines from ^{128}Te, ^{136}Ce and the 511 keV annihilation peak were used for calibration at low energy together with the ^{56}Co data for calibrating higher energies.

For particle detection, the SORCERER detector was used. SORCERER includes commercial solar cells as particle detectors. Si detectors for spectroscopy applications have better resolution than solar cells, but used with heavy-ion beams their resolution would degrade rapidly over the course of the experiment. The Si detectors would then lose their resolution due to crystal defects caused by the heavy ions. The degrading also happens to the solar cells, but because they are mass produced and much cheaper to replace, it is more feasible to replace them after each experiment with a heavy-ion beam. As the detectors degrade during the experiment, the detected energy drifts significantly. This requires either constant recalibration, or adapting the gating conditions over the course of the experiment. Instead of calibrating the spectra, we chose to find new appropriate gates every 20 runs (out of a total of 188 runs). This is illustrated in Fig 3.8.

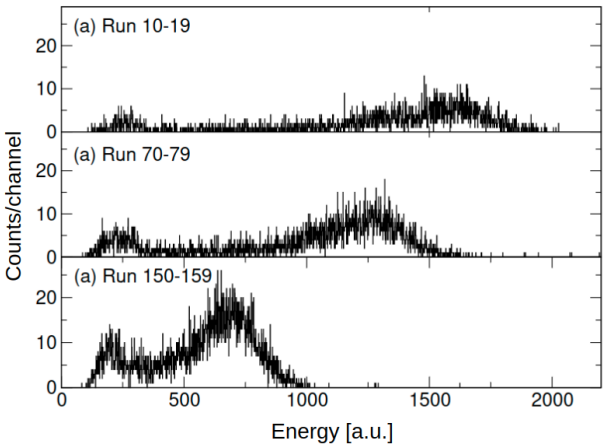

Figure 3.8: Particle spectra from SORCERER showing the degradation of the solar cell detectors over time. The spectra were produced by gating on the 1141 keV transition in a particle-γ coincidence matrix for different run times at the (a) beginning, (b) middle, and (c) end of the experiment. The energy is given in arbitrary units, and the Si energy gates were moved according to the new spectrum for every 20th run file.

3.2.2 Cleaning the spectra

Even though the ^{18}O beam contains two neutrons outside the doubly magic ^{16}O core, the two-neutron transfer reaction was not the strongest transfer reaction in the experiment. As shown in the γ-ray singles spectra in Paper IV, there are many events from ^{128}Te created by α transfer. Instead of transferring the two neutrons outside the ^{16}O core, the reaction channel for transferring a tightly bound α core is in other words stronger. There are also many γ rays from ^{138}Ce, created by fusion evaporation where the incident beam fusions with the target and emits four neutrons. Although a relatively low beam energy just below the Coulomb barrier was chosen, the sub-barrier fusion cross section was of similar magnitude as the two-neutron transfer cross section. In addition to these reactions, there is also in general a large Compton background, making the initial γ ray spectra crowded with many transitions that are not of interest.

Several steps were taken to clean the spectra by selecting events of interest and suppressing events from contaminations. Figure 1 in Paper IV shows the Si particle detector energy spectrum for particles detected in coincidence with γ rays. The low-energy peak is mostly due to events from light particles and electronic noise. The neutrons emitted in the fusion-evaporation reaction do not produce a signal in the Si detectors, and are not seen in the spectrum. The ^{16}O and ^{14}C ejectiles from the two-neutron and α transfer reactions produce a large signal. Because the Si detectors cover a large range of scattering angles, but with relatively poor resolution, the signals from detecting ^{16}O and ^{14}C overlap with each other and it is not possible to make a clean selection. However, gating on prompt coincidences between γ detection in ROSPHERE and high-energy events in SORCERER largely suppresses fusion-evaporation events, as is illustrated in Figure 1 of Paper IV. In addition, a gate on the time spectrum showing the time between a detected particle and γ event could be chosen to exclude random events. The final gates regards

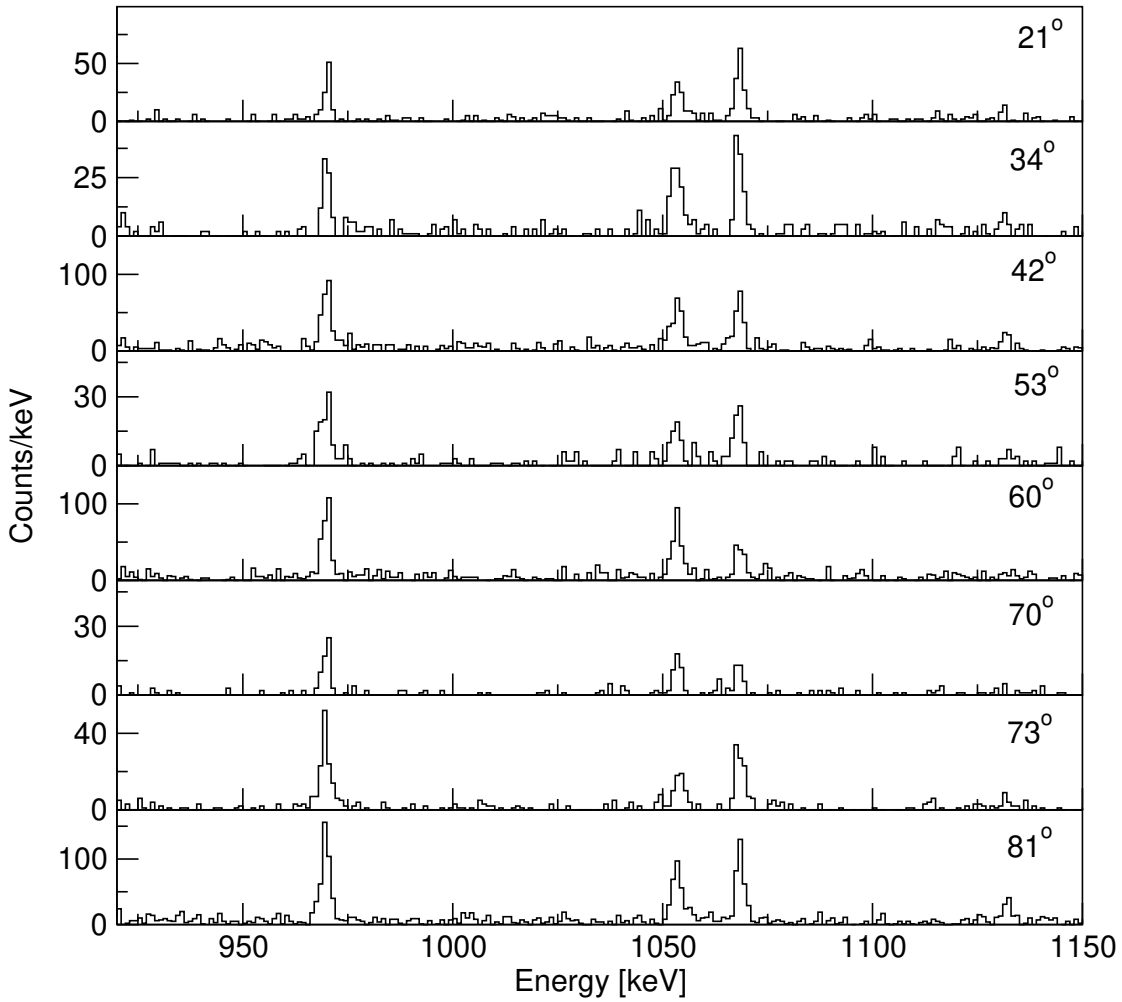

Figure 3.9: Gates on the 1141 keV peak for different angles relative to the direction of the 1141 keV γ ray, showing the change in relative sizes of the peaks originating from states of different spins.

the BGO shielding. The Compton suppression was performed in software, where signals from the HPGe and BGO detectors were recorded separately, and events where a Ge detector and a surrounding BGO detector gave coincident signals were suppressed in the data sorting.

3.2.3 Angular correlations

Figure 3.9 shows γ-γ coincidence spectra gated on the 1141 keV transition for the different detector angles. This illustrates how the relative size of the 1053 and 1068 keV peaks changes with the detection angle relative to the direction of the 1141 keV γ ray. By measuring the areas of these peaks, and the 909 keV peak used for normalisation, the angular correlation could be obtained, with the results as presented in Paper IV.

Chapter 4

Future Work

4.1 lifetime measurements

One of the original goals of the ^{126}Sn experiment was to measure lifetimes with two different methods, the Doppler-Shift Attenuation Method (DSAM) and the Recoil-Distance Doppler Shift(RDDS) method. The DSAM uses a thick target in which the recoil is stopped. Transitions from very short-lived states well below 1 ps produce characteristic line shapes if detected under forward and backward angles from the change in Doppler shift as the recoils are being stopped in the thick target. By comparing the experimental line shapes with simulations of the stopping process, the lifetime of the state can be related to the time it takes to stop the recoils [42]. The RDDS method uses a thin target and a stopper foil with a variable distance in the micrometer range between the two foils. If the lifetime of the state is of the order of the flight time between the target and the stopper, a transition will be split into a Doppler-shifted and a stopped component. By measuring the intensity of the two components as a function of distance, lifetimes in the range between 1 ps and a few hundred ps can be measured [43]. The experimental equipment at IFIN-HH is ideal for both methods, and the SORCERER detector was designed with these types of experiments in mind. The present experiment used a thick target, so the DSAM can in principle be applied. For an RDDS measurement, the thick target needs to be replaced by a thin target and a stopper foil in a device that allows controlling the distance, a so-called *plunger*. Figure 4.10 shows spectra for selected transitions in ^{124}Sn and ^{126}Sn, and how their line-shapes are affected by their lifetimes. Spectra a) and b) are gated on the 1131 keV transition in ^{124}Sn and show the 1471 keV transition originating from the 3^- state observed under forward (37^o) angles. The state has a known half-life of 68(6) fs [44]. Because of the extremely short lifetime, which is much shorter than the stopping time, the γ ray is largely emitted with the full Doppler shift, resulting in the large Doppler shifted peaks. Spectra c) and d) show the corresponding 1574 keV transition from the 3^- state in ^{126}Sn after gating on the 1141 keV transition. The similar line shapes as compared to the 1471 keV transition suggest that the lifetime of the 3^- state in ^{126}Sn is similar to the one in ^{124}Sn. Spectra e) and f) show the 998 keV transition from the 2_2^+ state in ^{124}Sn, which has a half-life of 0.8 (+0.5,-0.2) ps [45]. This much longer half-life is at the upper end of sensitivity range

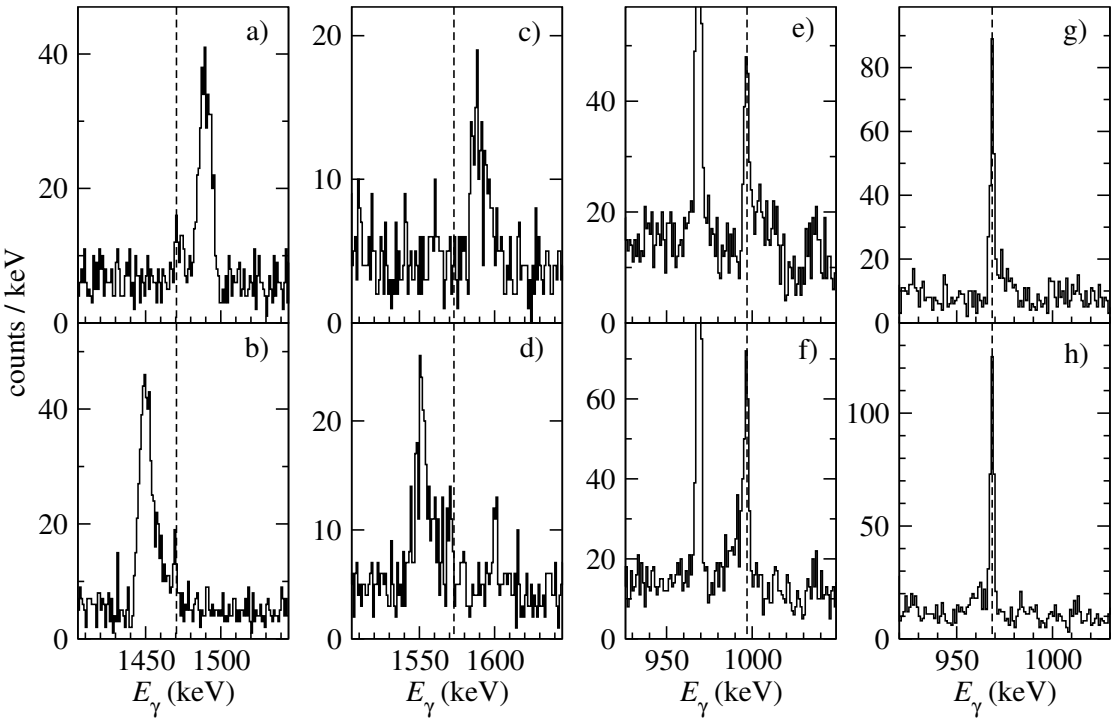

Figure 4.10: A look at different lifetimes that can be studied with the DSA method.

of the DSA method, where most of the recoils are stopped at the time of the γ emission. The few events where the recoils are still moving are responsible for the shoulders that are visible on the peak. Spectra g) and h) show the corresponding 970 keV transition from the 2_2^+ state in ^{126}Sn. Again the line shapes are very similar to the ^{124}Sn case, suggesting that the 2_2^+ states have similar lifetimes.

A similar phenomenon is also seen in the singles spectrum, as briefly mentioned in Paper IV, where the spread of the peak is caused by the characteristic line shapes of transitions from very short-lived states. By analysing the line-shapes and comparing them with simulations of the events, it is possible to use this to obtain lifetimes of states with currently unknown lifetimes. The lifetime of the new 0^+ state in ^{126}Sn is too long to be measured by the DSAM. This, together with time constraints of the PhD work, is the reason why a DSAM analysis was not included in Paper IV. Nevertheless, it will be possible to determine the lifetime of the 3^- and 2_2^+ states, which will be the subject of another publication in the future.

For lifetimes in the ps range, the RDDS method can be applied with a plunger setup using a thin target. Originally it was planned to mount a plunger setup after sufficient amount of data was collected with the thick target. Unfortunately, making a sufficiently thin ^{124}Sn target that could be stretched onto a plunger frame was difficult, and this part of the experiment was rather unsuccessful. Different ^{124}Sn targets were produced by evaporating ^{124}Sn onto a thin Au backing. The Au backing was necessary in order to stretch the target, producing a smooth surface, and was facing the beam. The thick stopper foil was also made of Au. Making the Sn target thin enough to perform the plunger method, while not breaking, was not possible. The thinnest versions of these targets broke shortly after being hit

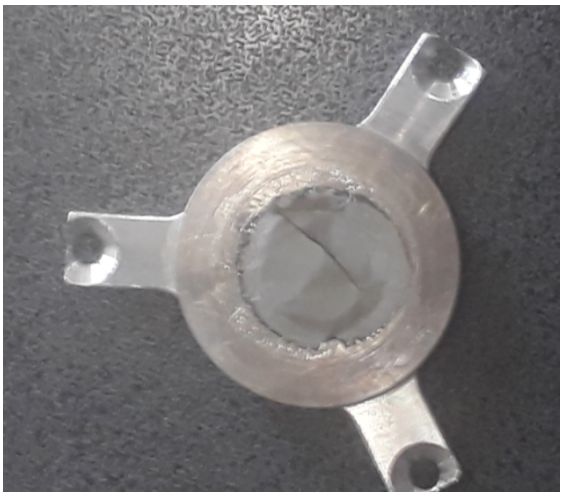

Figure 4.11: One of the thin ^{124}Sn targets, that was mounted and stretched onto a plunger frame, but later broke.

by the beams, as seen in Figure 4.11. The thicker versions did not break, but did not produce enough events of interest compared to the background events, which were dominated by Coulomb excitation of Au in the target backing and stopper foil. A spectrum from the thicker version of the plunger is shown in Figure 4.12.

Another method to measure the longer half-lives in ^{126}Sn that can be applied in future experiments would be to use different γ detectors like LaBr3(Ce) with better time resolution than the HPGe detectors. With this setup, lifetimes longer than 20-30 ps can be measured directly [46]. The ROSPHERE detector array can be reconfigured to contain both high-resolution HPGe and fast LaBr3(Ce) detectors.

MCSM calculations similar to the ones done for the Cu isotopes under study are also planned to be performed for ^{126}Sn. If the calculations also produce a 0^+ excited state at a similar energy as the one seen experimentally, this can be used to better characterise the nature of the excitation. By studying the shell model configuration and shape analysis of the 0^+ state, it can be discussed in more detail whether this indeed is a deformed intruder state or not. A comparison of calculated $B(E2; 0_2^+ \rightarrow 2_1^+)$ transition strength with an experimental value would be very helpful, and a new attempt to measure the lifetime would be useful.

4.2 Current and future work in the ^{78}Ni region

Research on the neutron rich Cu isotopes is ongoing. An experiment using the proton knock-out reaction to study the odd-even ^{75,77}Cu isotopes was performed at RIKEN under the SEASTAR experiment [47]. The previously mentioned proton core-excited states are strongly populated in the ^{76,78}Zn$(p, 2p)^{75,77}$Cu reactions, and the comparison of experimental and theoretical cross sections could help to identify these states. The identification of core-excited states in the neutron-rich Cu isotopes will also shed more light on shape coexistence in the Ni isotopes, as illustrated earlier in Figure 1.5.

More research is required in order to properly understand the nature of

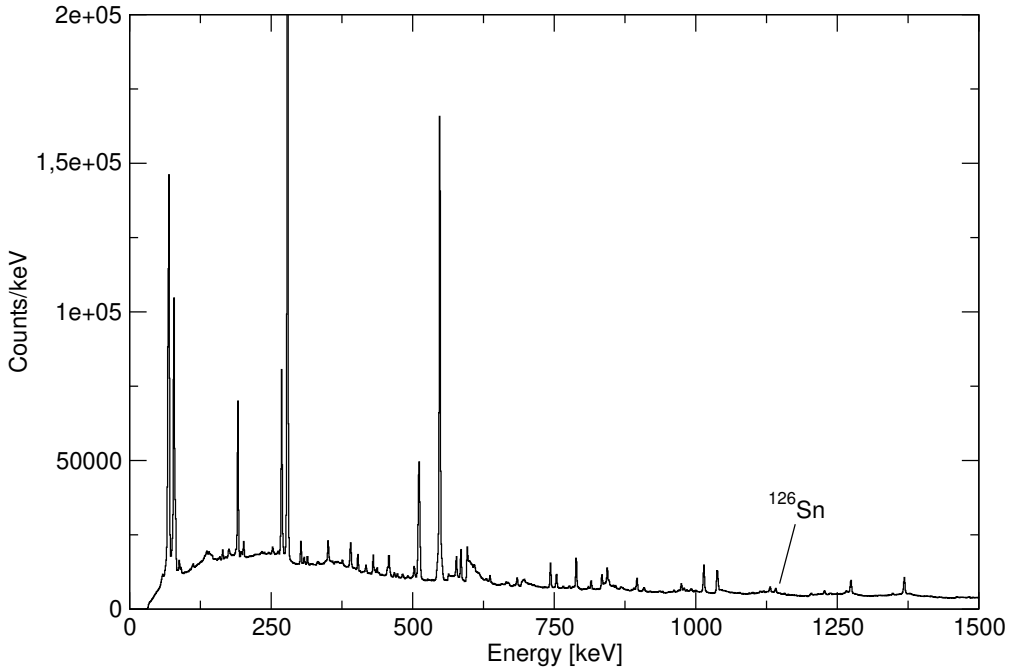

Figure 4.12: Total projection of the $\gamma\gamma$ matrix obtained after 24 hours of data taking with the plunger setup. The spectrum is gated on particles detected in SORCERER. The 1141 keV peaks from ^{126}Sn is highlighted to show its size compared to γ rays from the Coulomb excitation of Au.

the excited states in both the odd-even and odd-odd Cu isotopes. Lifetime measurements in the Cu isotopes under study can be used to further understand the structure of the newly observed states. A new experiment to measure lifetimes in Cu has been proposed at RIKEN. It will use the same technique as the experiments described in Papers I-III, but the EURICA HPGe detectors will be replaced by a large array of fast LaBr3(Ce) detectors, which allow measuring lifetimes above approximately 30 ps using the fast-timing technique [48, 49].

A total absorption spectroscopy study can be used to assign spin for more of the excited states. Spin assignments have been difficult in the present work because of unobserved feeding, which makes determining $\log ft$ values very challenging. In a total absorption experiment, the β-decaying nuclides are stopped inside a large 4π γ-ray detector, ensuring that all γ-ray events are detected. Total absorption spectroscopy can be used to determine the precise amount of β feeding into the various excited states [50]. The combination of high-resolution discrete spectroscopy and total-absorption spectroscopy is therefore powerful and necessary for a more precise β-feeding analysis, which is needed for more complete spin assignments. In these experiments, the issues with missing feeding to the different states are eliminated and the feeding, and thus also $\log ft$ values and spin assignments, are much less speculative.

A total absorption experiment would be particularly useful if a segmented TAS was used. In this case the total detected energy determines the excitation energy of the nucleus, while it is still possible to detect individual γ rays. This allows applying the so-called β-Oslo method to determine the level density and

γ-ray strength function [51]. These quantities are crucial ingredients to calculate neutron-capture cross sections [52]. This can further be used to find the neutron capture rates, and thus also improve astrophysical calculations. A sensitivity study [53] found especially the neutron-capture rate of ^{76}Cu to be important in such calculations. A natural next step for these nuclei will be to perform β-Oslo method type experiments on these nuclei when this is experimentally accessible.

This thesis presents the first spectroscopy results for the most neutron-rich odd-odd Cu isotopes studied so far. Especially the results of ^{78}Cu provided important information on the proton-neutron interaction only one neutron away from the closed shell $N = 50$. Continuing the research on neutron-rich odd-odd Cu isotopes, the next in line is ^{80}Cu. Very little is known about this nucleus, but its half-life at 0.17 (+11,-5) s is measured [54]. In future experiments where more events are created and detected, together with detecting emitted γ rays, a similar study can be applied to this nucleus as well. While the current study of ^{78}Cu revealed the mechanics of particle-hole dynamics, a similar study of ^{80}Cu will give greater insight into the proton-neutron interaction with particle-particle coupling between the $\pi f_{5/2}$ and $\nu d_{5/2}$ orbitals. This will give further insight into the structure beyond the $N = 50$ shell closure, and will be useful for further shell model calculation codes and an important step into the study of the structural changes in the Cu isotopic chain towards the neutron drip line.

Bibliography

[1] Kenneth S Krane. *Introductory nuclear physics*. New York, NY: Wiley, 1988.

[2] Maria G. Mayer. 'On Closed Shells in Nuclei'. In: *Phys. Rev.* 74 (3 Aug. 1948), pp. 235–239. DOI: 10.1103/PhysRev.74.235. URL: https://link.aps.org/doi/10.1103/PhysRev.74.235.

[3] Maria Goeppert Mayer. 'On Closed Shells in Nuclei. II'. In: *Phys. Rev.* 75 (12 June 1949), pp. 1969–1970. DOI: 10.1103/PhysRev.75.1969. URL: https://link.aps.org/doi/10.1103/PhysRev.75.1969.

[4] A. Navin et al. 'Direct Evidence for the Breakdown of the $N = 8$ Shell Closure in ^{12}Be'. In: *Phys. Rev. Lett.* 85 (2 July 2000), pp. 266–269. DOI: 10.1103/PhysRevLett.85.266. URL: https://link.aps.org/doi/10.1103/PhysRevLett.85.266.

[5] T. Motobayashi et al. 'Large deformation of the very neutron-rich nucleus 32Mg from intermediate-energy Coulomb excitation'. In: *Physics Letters B* 346.1 (1995), pp. 9–14. ISSN: 0370-2693. DOI: https://doi.org/10.1016/0370-2693(95)00012-A. URL: https://www.sciencedirect.com/science/article/pii/037026939500012A.

[6] B. Bastin et al. 'Collapse of the $N = 28$ Shell Closure in ^{42}Si'. In: *Phys. Rev. Lett.* 99 (2 July 2007), p. 022503. DOI: 10.1103/PhysRevLett.99.022503. URL: https://link.aps.org/doi/10.1103/PhysRevLett.99.022503.

[7] D. Steppenbeck et al. 'Evidence for a new nuclear 'magic number' from the level structure of 54Ca'. In: *Nature* 502.7470 (Oct. 2013), pp. 207–210. ISSN: 1476-4687. DOI: 10.1038/nature12522. URL: https://doi.org/10.1038/nature12522.

[8] Takaharu Otsuka et al. 'Evolution of Nuclear Shells due to the Tensor Force'. In: *Phys. Rev. Lett.* 95 (23 Nov. 2005), p. 232502. DOI: 10.1103/PhysRevLett.95.232502. URL: https://link.aps.org/doi/10.1103/PhysRevLett.95.232502.

[9] V. Paar. 'A parabolic rule for the energy dependence on x = I(I + 1) for proton-neutron multiplets in odd-odd nuclei'. In: *Nuclear Physics A* 331.1 (1979), pp. 16–28. ISSN: 0375-9474. DOI: https://doi.org/10.1016/0375-9474(79)90297-5. URL: https://www.sciencedirect.com/science/article/pii/0375947479902975.

[10] O. Sorlin and M.-G. Porquet. 'Nuclear magic numbers: New features far from stability'. In: *Progress in Particle and Nuclear Physics* 61.2 (2008), pp. 602–673. ISSN: 0146-6410. DOI: https://doi.org/10.1016/j.ppnp.2008.05.001. URL: https://www.sciencedirect.com/science/article/pii/S0146641008000380.

[11] K. T. Flanagan et al. 'Nuclear Spins and Magnetic Moments of ^{71,73,75}Cu: Inversion of $\pi 2p_{3/2}$ and $\pi 1f_{5/2}$ Levels in ^{75}Cu'. In: *Phys. Rev. Lett.* 103 (14 Oct. 2009), p. 142501. DOI: 10.1103/PhysRevLett.103.142501. URL: https://link.aps.org/doi/10.1103/PhysRevLett.103.142501.

[12] E. Sahin et al. 'Shell Evolution towards ^{78}Ni: Low-Lying States in ^{77}Cu'. In: *Phys. Rev. Lett.* 118 (24 June 2017), p. 242502. DOI: 10.1103/PhysRevLett.118.242502. URL: https://link.aps.org/doi/10.1103/PhysRevLett.118.242502.

[13] F. L. Bello Garrote et al. 'β decay of ^{75}Ni and the systematics of the low-lying level structure of neutron-rich odd-A Cu isotopes'. In: *Phys. Rev. C* 102 (3 Sept. 2020), p. 034314. DOI: 10.1103/PhysRevC.102.034314. URL: https://link.aps.org/doi/10.1103/PhysRevC.102.034314.

[14] Eda Sahin. Private communications.

[15] S.E. Koonin, D.J. Dean and K. Langanke. 'Shell model Monte Carlo methods'. In: *Physics Reports* 278.1 (1997), pp. 1–77. ISSN: 0370-1573. DOI: https://doi.org/10.1016/S0370-1573(96)00017-8. URL: https://www.sciencedirect.com/science/article/pii/S0370157396000178.

[16] Takaharu Otsuka et al. 'Magic Numbers in Exotic Nuclei and Spin-Isospin Properties of the NN Interaction'. In: *Phys. Rev. Lett.* 87 (8 Aug. 2001), pp. 082502–1.

[17] Noritaka Shimizu et al. 'New-generation Monte Carlo shell model for the K computer era'. In: *Progress of Theoretical and Experimental Physics* 2012.1 (Sept. 2012), 01A205. ISSN: 2050-3911. DOI: 10.1093/ptep/pts012. eprint: https://academic.oup.com/ptep/article-pdf/2012/1/01A205/11585951/pts012.pdf. URL: https://doi.org/10.1093/ptep/pts012.

[18] Kris Heyde and John L. Wood. 'Shape coexistence in atomic nuclei'. In: *Rev. Mod. Phys.* 83 (4 Nov. 2011), pp. 1467–1521. DOI: 10.1103/RevModPhys.83.1467. URL: https://link.aps.org/doi/10.1103/RevModPhys.83.1467.

[19] Paul E. Garrett, Magda Zielińska and Emmanuel Clément. 'An experimental view on shape coexistence in nuclei'. In: *Progress in Particle and Nuclear Physics* 124 (2022), p. 103931. ISSN: 0146-6410. DOI: https://doi.org/10.1016/j.ppnp.2021.103931. URL: https://www.sciencedirect.com/science/article/pii/S0146641021000922.

[20] H.W. Fielding et al. 'O+ states observed in Cd and Sn nuclei with the (3He, n) reaction'. In: *Nuclear Physics A* 281.3 (1977), pp. 389–404. ISSN: 0375-9474. DOI: https://doi.org/10.1016/0375-9474(77)90504-8. URL: https://www.sciencedirect.com/science/article/pii/0375947477905048.

[21] David J. Rowe and John L. Wood. *Fundementals of Nuclear Models: Foundational Models*. Wspc, 2010.

[22] P.-A. Söderström et al. 'Installation and commissioning of EURICA – Euroball-RIKEN Cluster Array'. In: *Nuclear Instruments and Methods in Physics Research Section B: Beam Interactions with Materials and Atoms* 317 (2013). XVIth International Conference on ElectroMagnetic Isotope Separators and Techniques Related to their Applications, December 2–7, 2012 at Matsue, Japan, pp. 649–652. ISSN: 0168-583X. DOI: https://doi.org/10.1016/j.nimb.2013.03.018. URL: https://www.sciencedirect.com/science/article/pii/S0168583X13003182.

[23] https://ribf.riken.jp/EURICA/. 2016.

[24] J. Eberth et al. 'Encapsulated Ge detectors: Development and first tests'. In: *Nuclear Instruments and Methods in Physics Research Section A: Accelerators, Spectrometers, Detectors and Associated Equipment* 369.1 (1996), pp. 135–140. ISSN: 0168-9002. DOI: https://doi.org/10.1016/0168-9002(95)00794-6. URL: https://www.sciencedirect.com/science/article/pii/0168900295007946.

[25] *Achievements with the EUROBALL spectrometer*. http://euroball.lnl.infn.it/. 2003.

[26] Z. Y. Xu. 'Beta-decay spectroscopy on neutron-rich nuclei in a range of Z = 26 - 32'. PhD thesis. Department of Physics, University of Tokyo, 2014. URL: http://hdl.handle.net/2261/57714.

[27] Z. Y. Xu et al. 'β-Decay Half-Lives of ^{76,77}Co, ^{79,80}Ni, and ^{81}Cu: Experimental Indication of a Doubly Magic ^{78}Ni'. In: *Phys. Rev. Lett.* 113 (3 July 2014), p. 032505. DOI: 10.1103/PhysRevLett.113.032505. URL: https://link.aps.org/doi/10.1103/PhysRevLett.113.032505.

[28] Toshiyuki Kubo et al. 'BigRIPS separator and ZeroDegree spectrometer at RIKEN RI Beam Factory'. In: *Progress of Theoretical and Experimental Physics* 2012.1 (Dec. 2012), p. 03C003. ISSN: 2050-3911. DOI: 10.1093/ptep/pts064. eprint: https://academic.oup.com/ptep/article-pdf/2012/1/03C003/11595011/pts064.pdf. URL: https://doi.org/10.1093/ptep/pts064.

[29] D.C. Radford. *Notes on the use of the program GF3*. May 2010. URL: https://radware.phy.ornl.gov/gf3/.

[30] Steffen Turkat et al. 'Systematics of logft values for β^-, and EC/β^+ transitions'. In: *Atomic Data and Nuclear Data Tables* 152 (2023), p. 101584. ISSN: 0092-640X. DOI: https://doi.org/10.1016/j.adt.2023.101584. URL: https://www.sciencedirect.com/science/article/pii/S0092640X23000128.

[31] M. Emeric and A. Sonzogni. *Logft calculator*. https://www.nndc.bnl.gov/logft/.

[32] J.C. Hardy et al. 'The essential decay of pandemonium: A demonstration of errors in complex beta-decay schemes'. In: *Physics Letters B* 71 (Nov. 1977), pp. 307–310. DOI: 10.1016/0370-2693(77)90223-4.

[33] J.L Wood et al. 'Coexistence in even-mass nuclei'. In: *Physics Reports* 215.3 (1992), pp. 101–201. ISSN: 0370-1573. DOI: https://doi.org/10.1016/0370-1573(92)90095-H. URL: https://www.sciencedirect.com/science/article/pii/037015739290095H.

[34] B. Fogelberg and P. Carlé. 'Levels and transition probabilities in 120, 122, 124, 126, 128sn studied in the decay of In isotopes'. In: *Nuclear Physics A* 323.2 (1979), pp. 205–252. ISSN: 0375-9474. DOI: https://doi.org/10.1016/0375-9474(79)90108-8. URL: https://www.sciencedirect.com/science/article/pii/0375947479901088.

[35] S. Leoni et al. 'Multifaceted Quadruplet of Low-Lying Spin-Zero States in ^{66}Ni: Emergence of Shape Isomerism in Light Nuclei'. In: *Phys. Rev. Lett.* 118 (16 Apr. 2017), p. 162502. DOI: 10.1103/PhysRevLett.118.162502. URL: https://link.aps.org/doi/10.1103/PhysRevLett.118.162502.

[36] D. Bucurescu et al. 'The ROSPHERE γ-ray spectroscopy array'. In: *Nuclear Instruments and Methods in Physics Research Section A: Accelerators, Spectrometers, Detectors and Associated Equipment* 837 (2016), pp. 1–10. ISSN: 0168-9002. DOI: https://doi.org/10.1016/j.nima.2016.08.052. URL: https://www.sciencedirect.com/science/article/pii/S0168900216308798.

[37] T. Beck et al. 'SORCERER: A novel particle-detection system for transfer-reaction experiments at ROSPHERE'. In: *Nuclear Instruments and Methods in Physics Research Section A: Accelerators, Spectrometers, Detectors and Associated Equipment* 951 (2020), p. 163090. ISSN: 0168-9002. DOI: https://doi.org/10.1016/j.nima.2019.163090. URL: https://www.sciencedirect.com/science/article/pii/S0168900219314299.

[38] H.W. Taylor et al. 'A tabulation of gamma-gamma directional-correlation coefficients'. In: *Atomic Data and Nuclear Data Tables* 9.1 (1971), pp. 1–83. ISSN: 0092-640X. DOI: https://doi.org/10.1016/S0092-640X(71)80040-2. URL: https://www.sciencedirect.com/science/article/pii/S0092640X71800402.

[39] TRIUMF. *Angular Correlation Calculator*. 2015. DOI: 10.5281/zenodo.45587. URL: http://griffincollaboration.github.io/AngularCorrelationUtility/.

[40] Simon Giraud. 'Mesures de masse autour du 78Ni et nouveau traitement de l'équilibre statistique nucléaire pour l'étude des supernovae à effondrement de coeur'. Theses. Normandie Université, Sept. 2019. URL: https://theses.hal.science/tel-03354941.

[41] S. Giraud et al. 'Mass measurements towards doubly magic 78Ni: Hydrodynamics versus nuclear mass contribution in core-collapse supernovae'. In: *Physics Letters B* 833 (2022), p. 137309. ISSN: 0370-2693. DOI: https://doi.org/10.1016/j.physletb.2022.137309. URL: https://www.sciencedirect.com/science/article/pii/S0370269322004439.

[42] T. K. Alexander and J. S. Forster. 'Lifetime Measurements of Excited Nuclear Levels by Doppler-Shift Methods'. In: *Advances in Nuclear Physics: Volume 10*. Ed. by Michel Baranger and Erich Vogt. Boston, MA: Springer US, 1978, pp. 197–331. ISBN: 978-1-4757-4401-9. DOI: 10.1007/978-1-4757-4401-9_3. URL: https://doi.org/10.1007/978-1-4757-4401-9_3.

[43] A. Dewald, O. Möller and P. Petkov. 'Developing the Recoil Distance Doppler-Shift technique towards a versatile tool for lifetime measurements of excited nuclear states'. In: *Progress in Particle and Nuclear Physics* 67.3 (2012), pp. 786–839. ISSN: 0146-6410. DOI: https://doi.org/10.1016/j.ppnp.2012.03.003. URL: https://www.sciencedirect.com/science/article/pii/S0146641012000713.

[44] L. I. Govor et al. 'Lifetime Measurements for Excited ^{116,124}Sn States in the (n, n'γ) Reaction'. In: *Yad.Fiz.* 54 (1991), p. 330.

[45] D. Bandyopadhyay et al. 'Three-phonon excitations in 124Sn'. In: *Nuclear Physics A* 747.2 (2005), pp. 206–226. ISSN: 0375-9474. DOI: https://doi.org/10.1016/j.nuclphysa.2004.10.003. URL: https://www.sciencedirect.com/science/article/pii/S0375947404010814.

[46] J.-M. Régis et al. 'The mirror symmetric centroid difference method for picosecond lifetime measurements via γ–γ coincidences using very fast LaBr3(Ce) scintillator detectors'. In: *Nuclear Instruments and Methods in Physics Research Section A: Accelerators, Spectrometers, Detectors and Associated Equipment* 622.1 (2010), pp. 83–92. ISSN: 0168-9002. DOI: https://doi.org/10.1016/j.nima.2010.07.047. URL: https://www.sciencedirect.com/science/article/pii/S0168900210016578.

[47] Sahin, E. et al. 'Probing the nuclear structure in the vicinity of 78Ni'. In: *EPJ Web Conf.* 223 (2019), p. 01054. DOI: 10.1051/epjconf/201922301054. URL: https://doi.org/10.1051/epjconf/201922301054.

[48] H. Mach, R.L. Gill and M. Moszyński. 'A method for picosecond lifetime measurements for neutron-rich nuclei: (1) Outline of the method'. In: *Nuclear Instruments and Methods in Physics Research Section A: Accelerators, Spectrometers, Detectors and Associated Equipment* 280.1 (1989), pp. 49–72. ISSN: 0168-9002. DOI: https://doi.org/10.1016/0168-9002(89)91272-2. URL: https://www.sciencedirect.com/science/article/pii/0168900289912722.

[49] J.-M. Régis et al. 'The generalized centroid difference method for picosecond sensitive determination of lifetimes of nuclear excited states using large fast-timing arrays'. In: *Nuclear Instruments and Methods in Physics Research Section A: Accelerators, Spectrometers, Detectors and Associated Equipment* 726 (2013), pp. 191–202. ISSN: 0168-9002. DOI: https://doi.org/10.1016/j.nima.2013.05.126. URL: https://www.sciencedirect.com/science/article/pii/S0168900213007377.

[50] B Rubio et al. 'Beta decay studies with total absorption spectroscopy and the Lucrecia spectrometer at ISOLDE*'. In: *Journal of Physics G: Nuclear and Particle Physics* 44.8 (June 2017), p. 084004. DOI: 10.1088/1361-6471/aa797f. URL: https://dx.doi.org/10.1088/1361-6471/aa797f.

[51] A. Spyrou et al. 'Novel technique for Constraining r-Process (n, γ) Reaction Rates'. In: *Phys. Rev. Lett.* 113 (23 Dec. 2014), p. 232502. DOI: 10.1103/PhysRevLett.113.232502. URL: https://link.aps.org/doi/10.1103/PhysRevLett.113.232502.

[52] A.C. Larsen et al. 'Novel techniques for constraining neutron-capture rates relevant for r-process heavy-element nucleosynthesis'. In: *Progress in Particle and Nuclear Physics* 107 (2019), pp. 69–108. ISSN: 0146-6410. DOI: https://doi.org/10.1016/j.ppnp.2019.04.002. URL: https://www.sciencedirect.com/science/article/pii/S0146641019300298.

[53] R. Surman et al. 'Sensitivity studies for the weak r process: neutron capture rates'. In: *AIP Advances* 4.4 (Feb. 2014), p. 041008. DOI: 10.1063/1.4867191. eprint: https://pubs.aip.org/aip/adv/article-pdf/doi/10.1063/1.4867191/12948222/041008_1_online.pdf. URL: https://doi.org/10.1063/1.4867191.

[54] M. Wang et al. 'The AME2012 atomic mass evaluation (II). Tables, graphs and references'. In: *Chin.Phys.C* 36 (2012), p. 1603.